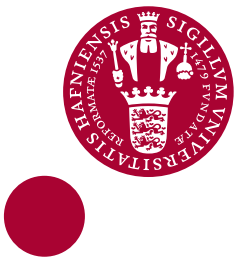

Noise Induces Hopping between NF-kappa B Entrainment Modes

Heltberg, Mathias; Kellogg, Ryan A.; Krishna, Sandeep; Tay, Savas; Jensen, Mogens H.

Published in:
Cell Systems

DOI:
10.1016/j.cels.2016.11.014

Publication date:
2016

Document version
Publisher's PDF, also known as Version of record

Article

Cell Systems

Noise Induces the Population-Level Entrainment of Incoherent, Uncoupled Intracellular Oscillators

Graphical Abstract

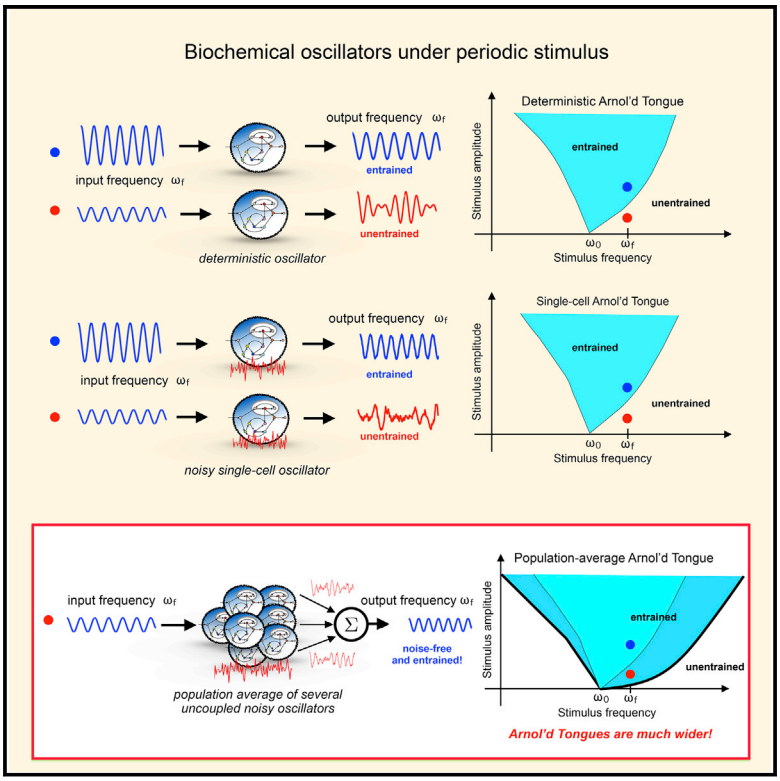

Highlights

- Intracellular oscillators often need to entrain to periodic stimuli
- However, biochemical noise can disrupt the entrainment of individual oscillators
- We show that population averages of noisy uncoupled oscillators entrain robustly
- This may explain how noisy peripheral clocks entrain nicely at the tissue level

Authors

Ankit Gupta, Benjamin Hepp, Mustafa Khammash

Correspondence

mustafa.khammash@bsse.ethz.ch

In Brief

Gupta et al. show that intrinsic biochemical noise can interact with dynamic nonlinearities to cause entrainment of the population mean of uncoupled intracellular oscillators, even though these oscillators may not be individually entrained. They call this effect stochastic population entrainment (SPE), and they demonstrate it both theoretically and computationally.

Gupta et al., 2016, Cell Systems 3, 521–531
December 21, 2016
http://dx.doi.org/10.1016/j.cels.2016.10.006

Cell Systems
Article

Noise Induces the Population-Level Entrainment of Incoherent, Uncoupled Intracellular Oscillators

Ankit Gupta,[1,2] Benjamin Hepp,[1,2] and Mustafa Khammash[1,3,*]
[1]Department of Biosystems Science and Engineering (D-BSSE), ETH-Zürich, Mattenstrasse 26, 4058 Basel, Switzerland
[2]Co-first author
[3]Lead Contact
*Correspondence: mustafa.khammash@bsse.ethz.ch
http://dx.doi.org/10.1016/j.cels.2016.10.006

SUMMARY

Intracellular oscillators entrain to periodic signals by adjusting their phase and frequency. However, the low copy numbers of key molecular players make the dynamics of these oscillators intrinsically noisy, disrupting their oscillatory activity and entrainment response. Here, we use a combination of computational methods and experimental observations to reveal a functional distinction between the entrainment of individual oscillators (e.g., inside cells) and the entrainment of populations of oscillators (e.g., across tissues). We demonstrate that, in the presence of intracellular noise, weak periodic cues robustly entrain the population averaged response, even while individual oscillators remain un-entrained. We mathematically elucidate this phenomenon, which we call stochastic population entrainment, and show that it naturally arises due to interactions between intrinsic noise and nonlinear oscillatory dynamics. Our findings suggest that robust tissue-level oscillations can be achieved by a simple mechanism that utilizes intrinsic biochemical noise, even in the absence of biochemical couplings between cells.

INTRODUCTION

Oscillators are known to play a large number of functional roles in biology (Vicker, 2002; Aulehla and Pourquié, 2008). For example, intracellular oscillators are responsible for generating circadian rhythms (Herzog et al., 2004), mounting immune (Tay et al., 2010) and stress responses (Batchelor et al., 2008), regulating signaling networks, and controlling cell proliferation (Cohen-Saidon et al., 2009). Generally, these oscillators are nonlinear (Pikovsky et al., 2001), and in the long run, their dynamics are constrained to a stable-limit cycle in state-space, that is, the space in which the trajectories lie. The periodic motion of the oscillator's state on this limit cycle can be described as a function of time t by $x(\omega_0 t + \phi_0)$, where x is a periodic function with period 2π, ω_0 is the natural frequency of the oscillator, and ϕ_0 is its phase. When such an oscillator is stimulated by a periodic forcing input (e.g., light in the case of circadian oscillators), it can lose its natural frequency and adopt the forcing frequency, ω_f, of the input and also lock its phase in a fixed relationship with the forcing input phase, transforming the dynamics from $x(\omega_0 t + \phi_0)$ to $x(\omega_f t + \phi_f)$. This phenomenon is called entrainment, and it has numerous physical, biological, and engineering applications (Pikovsky et al., 2001).

The most prominent example of a biological oscillator is a circadian clock that generates rhythms that are responsible for regulating a variety of physiological processes for a wide range of organisms (Reppert and Weaver, 2002). In mammals, the suprachiasmatic nucleus (SCN) of the hypothalamus is the dominant circadian pacemaker, but peripheral circadian clocks are present throughout the body (Brown et al., 2002). The SCN clock gets constantly entrained by the day's light/dark cycles and this helps in maintaining robust rhythmicity with a period of almost exactly 24 hr (Bagheri et al., 2008). Furthermore, the circadian rhythms produced by SCN subsequently entrain the peripheral circadian clocks that reside in various tissues throughout a mammalian body (Albrecht, 2012). These peripheral clocks then coordinate other cellular processes and drive many physiological functions in their respective tissues (Richards and Gumz, 2012). Hence, the phenomenon of entrainment plays a crucial role in the normal functioning of an organism on many scales.

Like circadian clocks, many intracellular oscillatory circuits receive extracellular inputs, such as cytokine concentrations (Tay et al., 2010) or stress signals (Baker et al., 1984), which can be periodic (Han et al., 2012; Dolmetsch et al., 1998) perhaps due to various biological rhythms present in an organism. In these cases, entrainment can help the cells respond to the external periodic signal in a synchronized manner. Furthermore, recent work in single cells has uncovered many transcription factors that that exhibit periodic pulses in activity in the presence of constant extracellular inputs (Purvis and Lahav, 2013; Lin et al., 2015). These observations suggest that intracellular signaling dynamics may serve as entrainment cues for various genetic oscillators.

Oscillatory dynamics within cells are invariably affected by the random fluctuations or intrinsic noise that arises due to the involvement of molecular species with low copy numbers (Elowitz et al., 2002). This randomness creates cell-to-cell heterogeneity among identical cells, thereby enabling a population of cells to have a different dynamical behavior than individual cells. Therefore, it is important to study entrainment at both the single-cell level and at the bulk or the population level, where the output of several single cells is averaged. The latter context is biologically relevant because the population averaging may occur in vivo at the tissue level or in the bloodstream; it is conceivable that in comparison to the single-cell outputs, this averaged output has a more direct influence on the physiological processes of an organism. Without an entraining cue, it is known both experimentally and theoretically, that intrinsic noise

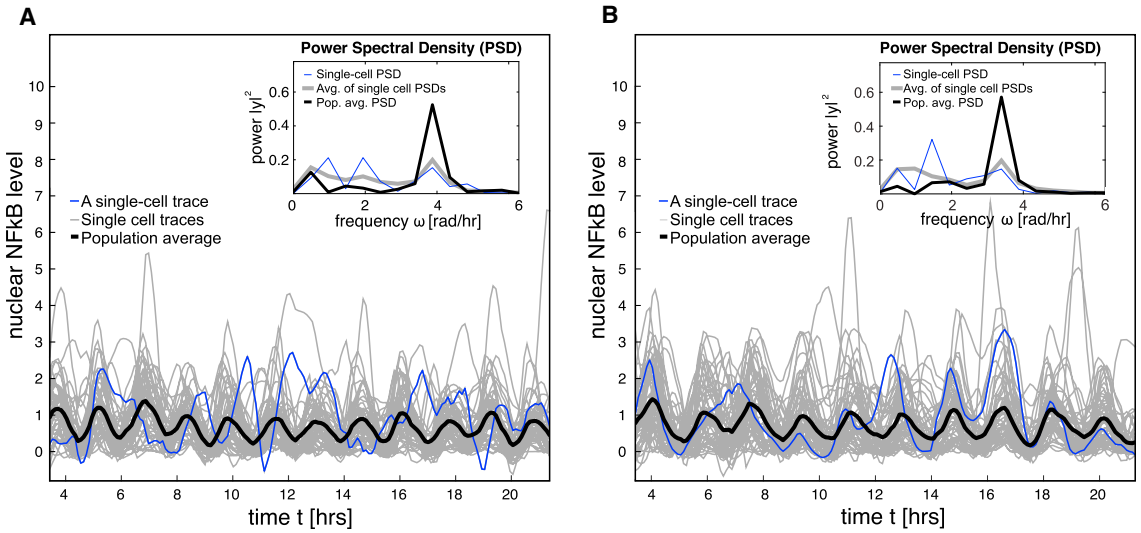

Figure 1. Single-Cell and Population-Average Dynamics of the NF-κB-TNFα System

(A and B) Analysis of the experimental data on NF-κB-TNF-α system reported in Kellogg and Tay (2015) with two input time periods: 90 (A) and 105 (B). These two input time periods represent forcing frequencies of $\omega_f = 2\pi/1.5\ hr^{-1}$ and $\omega_f = 2\pi/1.75\ hr^{-1}$. The natural frequency for this system is $\omega_0 = 2\pi/1.667\ hr^{-1}$ that corresponds to a time period of 100. For each input time period, we plot several single-cell trajectories (n = 52 in [A] and n = 58 [B], along with their average [black curve]). Only those single-cell trajectories are chosen from the sample that are not entrained to the input by themselves. Observe that the single-cell behavior is quite complex and incoherent, but the population-averaged dynamics oscillates nicely with a frequency very close to the forcing frequency ω_f. In the panel insets, we plot the normalized PSD (total power is 1) for a single-cell and the population average. We also display the average PSD of all the cells. These plots clearly show that unlike the single cells, the population-averaged trajectory puts most of its power at the forcing frequency ω_f and it entrains better than single-cell response to the periodic input.

can cause the oscillations of an individual oscillator or a single cell to be sloppy and incoherent (Welsh et al., 1995; Bagheri et al., 2008) to such an extent that phase variability among the cells becomes extreme, and the oscillatory activity is wiped out at the population level (Tay et al., 2010; Bagheri et al., 2008; Welsh et al., 1995; Aton et al., 2005). Even when an entraining periodic cue is present, we can expect intrinsic noise to hamper the entrainment response of single cells (Bagheri et al., 2008; Aton et al., 2005), but it has been unclear until now if the same effect will persist at the population level. The present study investigates this issue and demonstrates that intrinsic noise in fact benefits and even induces the population-level entrainment response.

RESULTS

This paper is motivated by an intriguing experimental discovery that we now describe. It is well known that the localization of the nuclear factor κB (NF-κB) transcription factor oscillates between the cytoplasm and the nucleus in response to treatment with extracellular cytokines such as tumor necrosis factor alpha (TNF-α) (Tay et al., 2010). In a recent work (Kellogg and Tay, 2015), microfluidics and time-lapse microscopy was used to study entrainment of this NF-κB-TNF-α system for several uncoupled single cells driven by a common input. The authors found that noise can improve as well as deteriorate the entrainment response of single cells, depending on the input signal's frequencies and strengths.

When we analyzed the experimental data presented in Kellogg and Tay (2015), we observed that if one averages several noisy single-cell signals, then the resulting population-level signal always entrains better to a periodic input. We illustrate this effect in Figure 1 that shows several noisy and incoherent single-cell traces along with their population average. Observe that unlike the single-cell traces, the population-level signal oscillates coherently with a frequency close to the input frequency ω_f, indicating that it is entrained. This is demonstrated by the power spectral density (Figure 1, inset) plots that show that the relative power assigned to the input frequency is small for the single-cell traces but large for the population-level signal. These analyses suggest that the population-averaged response of several uncoupled cells can entrain more easily than the individual oscillations of uncoupled single cells. Below, we provide computational and theoretical analyses that generalize these findings. We implicate intrinsic noise as the main cause for this enhancement of entrainment at the population level that we call stochastic population entrainment from now on. To the best of our knowledge, this beneficial effect of intrinsic noise has not been reported so far either experimentally or theoretically.

Characterization of Stochastic Population Entrainment in Three Contexts

The robustness of an oscillator's entrainment response can be identified with the area under its Arnol'd Tongue (Pikovsky et al., 2001; Mitarai et al., 2013) that plots the values of input amplitudes (A) and input frequencies (ω_f) for which the oscillator dynamics is entrained (Figure 2). Even though this concept is primarily defined for deterministic systems, we can appropriately modify it for stochastic systems (see the Quantification and Statistical Analysis section of the STAR Methods), which allows us to examine the role of intrinsic noise in population entrainment.

The first oscillator model we consider is the NF-κB signaling system (Krishna et al., 2006) that is activated by periodic TNF-α

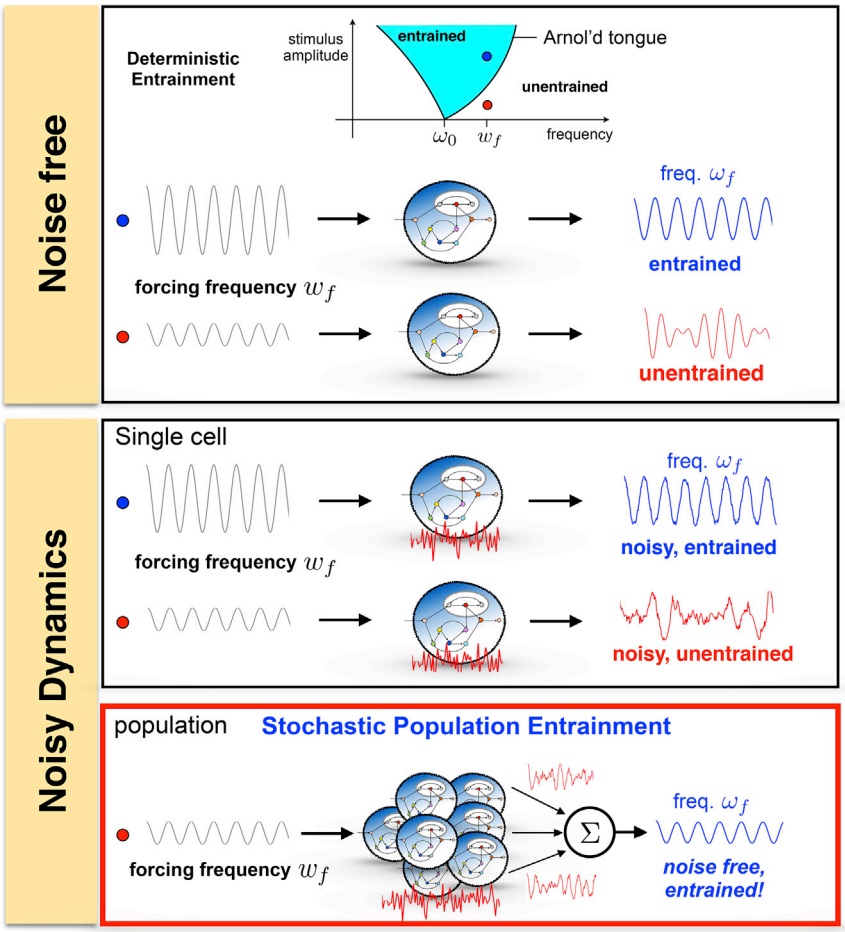

Figure 2. Illustration of Stochastic Population Entrainment

This figure illustrates the main finding of the paper. It considers an oscillator forced by a periodic input and compares its steady-state response in three scenarios: deterministic, single-cell, and population-level. The input frequency ω_f is close to the natural frequency ω_0 of the oscillator. Based on the deterministic Arnol'd Tongue (top), two amplitude values are selected that correspond to a weak input (red bubble) and a strong input (blue bubble), respectively. When intrinsic noise is present, the single-cell oscillations become sloppy but are similar to the deterministic case. In both these scenarios, the oscillator dynamics is not entrained (unentrained) if the input is weak, but it gets entrained if the input is strong. However, unlike these two scenarios, the population-level dynamics gets entrained even in the presence of weak input, suggesting that intrinsic noise can enhance the entrainment response at the population level.

inputs (see Figure 3A). This is a simple network consisting of five non-elementary reactions and three species: nuclear NF-κB, cytoplasmic IκB, and IκB mRNA. In the deterministic setting, the entrainment properties of this model were examined in Jensen and Krishna (2012). In the stochastic setting, the main source of intrinsic noise in the network is the transcription of IκB mRNA (Hayot and Jayaprakash, 2006). We approximate the noisy state dynamics $(x(t))_{t \geq 0}$ by a Langevin (Gillespie, 2000) stochastic differential equation (SDE) of the form:

$$\frac{dx}{dt} = F(x,t) + \Sigma(x,t)\xi(t), \qquad \text{(Equation 1)}$$

where $F(x,t)$ is the drift term, $\Sigma(x,t)$ is the diffusion matrix and $\xi(t)$ is the multi-dimensional white-noise process that captures the effects of intrinsic noise. The periodic input with frequency ω_f is noiseless (deterministic) and it appears in both $F(x,t)$ and $\Sigma(x,t)$, making them time-dependent functions that are periodic with frequency ω_f for a fixed state x. Solutions of this SDE gives us the single-cell traces that can be averaged (at each time point) to yield the population-level signal. To discern the effects of intrinsic noise, we also simulate the ordinary differential equation (ODE)

$$\frac{dx}{dt} = F(x,t), \qquad \text{(Equation 2)}$$

corresponding to the equivalent noise-free or deterministic model (Kurtz, 1978) of the network. We focus on dynamic heterogeneity, rather than heterogeneity in initial conditions, and we assume that all the cells start from the same initial condition. This implies that in the deterministic case, there is no source of cell-to-cell heterogeneity, and hence, the population-averaged response is the same as the response of a single cell. From Figure 3B, one can see that while the population-level signal oscillates coherently with a frequency close to the input frequency ω_f, the deterministic and the single-cell signals do not.

To judge the robustness of entrainment response, we numerically compute Arnol'd Tongues in all the three cases: single-cell, population-level, and deterministic. We find that in comparison to the deterministic case, the area of the single-cell Arnol'd Tongue shrinks by nearly 10% (see Figure 3C), but the area of the population-level Arnol'd Tongue expands by almost 50% (see Figure 3D). These results indicate that the presence of intrinsic noise makes the population-level entrainment response more robust than either the single-cell response or the deterministic response. Note that for any input frequency (close to the natural frequency), if the input amplitude is large relative to the natural amplitude of the oscillator, then all the three signals will entrain. Notably, our precise finding is that there exists a range of small amplitude values where only the population-level signal entrains but the other two signals do not (see the blue region in Figure 3D). Observe that all the three signals will coincide in the absence of intrinsic noise. Hence, the intrinsic noise induces the onset of entrainment at the population level, even though it may hinder it slightly at the individual level, as indicated by the shrinking Arnol'd Tongue in Figure 3C. This stochastic population entrainment effect suggests a functional role of intrinsic noise in the context of entrainment. For clarity, this phenomenon is illustrated as an idealized cartoon in Figure 2.

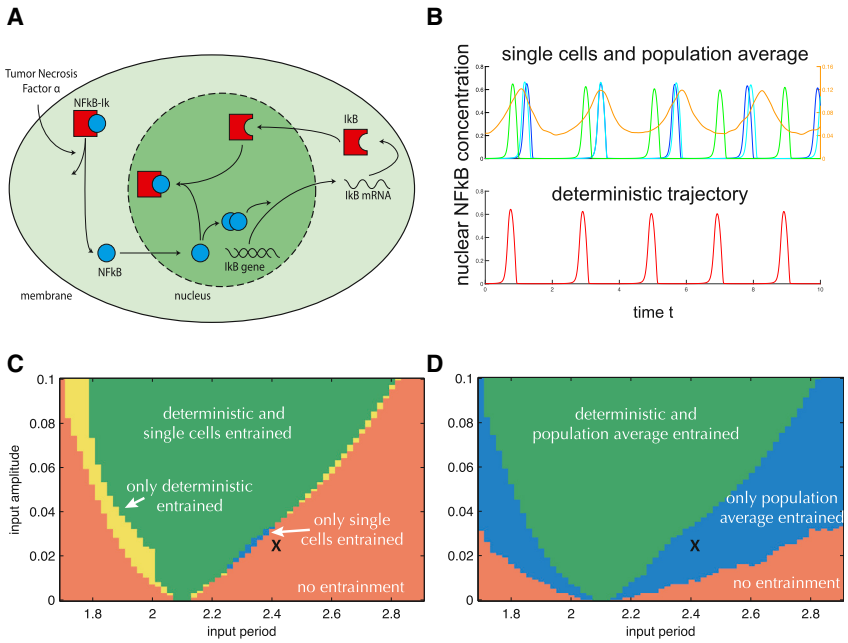

Figure 3. Stochastic Population Entrainment of the Spiky NF-κB Model

(A) Numerical results for the spiky NF-κB model (Krishna et al., 2006).

(B) Three single-cell trajectories (green, blue, and cyan), the population average of 10,000 trajectories (orange) and the corresponding deterministic trajectory. Note that this population average is calibrated with the second y axis is on the right, to show the oscillations more clearly. The values of input frequency and amplitude used for this simulation are marked with × in the Arnol'd Tongues below. From these plots it is evident that the single-cell trajectories are incoherent but similar to the deterministic trajectory, while the population-averaged trajectory oscillates regularly with a lower amplitude and with frequency ω_f.

(C) The entrainment regions (Arnol'd Tongues) for deterministic and single-cell cases are compared. These two tongues nearly overlap but there is a small region (yellow) where only the deterministic response entrains but the single-cell response does not.

(D) The Arnol'd Tongues for deterministic and population-level cases are compared, and one can clearly see that the population-level tongue is much broader. Specifically in the blue region, only the population-level signal entrains while the deterministic signal does not, again corroborating our main finding that intrinsic noise enhances entrainment at the population level. The Arnol'd Tongues are computed using 1,000 single-cell trajectories at each input frequency and amplitude.

Our analysis indicates that stochastic population entrainment can be expected to hold in two other biological oscillators that we now explore. First, we consider the detailed circadian clock model given in Leloup and Goldbeter (2003) with 16 species and 52 reactions (see Figure 4A). Here, the transcription of *Per* gene is modulated by the periodic light input and the resulting PER-mRNA is tracked as the output of the system. For this model, we simulate the full stochastic dynamics using Gillespie's algorithm (Gillespie, 1977), rather than using the SDE approximation for the dynamics as in the NF-κB example. This allows us to capture the low copy-number effects in the circadian clock dynamics more accurately.

In our analysis of this circadian clock, we observe in all three cases (single-cell, population-level, and deterministic) the signals (see Figure 4B) as well as the corresponding Arnol'd Tongues (see Figures 4C and 4D) are qualitatively similar to the NF-κB example. In comparison to the deterministic case, the area of the single-cell Arnol'd Tongue decreases by nearly 20% for this example, but the area of the population-level Arnol'd Tongue increases by more than 40%.

Second, we consider the classical Van der Pol oscillator (Pikovsky et al., 2001) that is used to model many physical and biological processes (Pikovsky et al., 2001). It is one of the simplest limit cycle oscillators and hence it has been extensively used in the study of oscillatory dynamics. Our analysis demonstrates that the Van der Pol model also exhibits stochastic population entrainment (see the Method Details section of the STAR Methods and Figure S1). Moreover, we performed a sensitivity check for this example by systematically perturbing the model parameters and computing the area under the associated Arnol'd Tongues. Our results show that the stochastic population entrainment effect is quite robust to perturbations in the model parameters (see the Method Details section of the STAR Methods and Table S1).

The Basis of Stochastic Population Entrainment

The role of noise in inducing entrainment, as we describe above for various oscillators, arises from the intricate interaction between noise and dynamics. This is elucidated using a simple heuristic example and rigorous mathematical analysis (see the Method Details section of the STAR Methods). We now outline the main ideas of this explanation. Suppose that the noise-free dynamics of a single cell under a constant forcing input, is given by an ordinary differential equation of the form of Equation 2 with some nonlinear time-invariant vector field $F(x,t) = F_0(x)$. We assume that this deterministic system admits a stable limit cycle and in the long run and its solutions move periodically on this limit cycle with natural frequency ω_0. Hence, for large values of t, we can express any solution as

$$x(t) \approx x_0(\omega_0 t + \phi_0), \qquad \text{(Equation 3)}$$

where x_0 is some 2π-periodic function and ϕ_0 is the initial phase. When intrinsic noise is present in the dynamics, it causes a phenomenon called phase diffusion (Pikovsky et al., 2001), whereby the solution trajectories diffuse like Brownian motion on the limit cycle, in addition to moving at the natural frequency ω_0. In this case, the dynamics can be represented by a stochastic differential equation of the form of Equation 1 and its solutions can be expressed as $x(t) \approx x_0(\omega_0 t + \phi_0(t))$. Here, $\phi_0(t)$ is a random variable that varies from cell to cell and it corresponds to the natural phase of the trajectory. We prove in the Method Details section of the STAR Methods that intrinsic noise has a phase-uniformization effect on the natural phase variable $\phi_0(t)$, which makes the

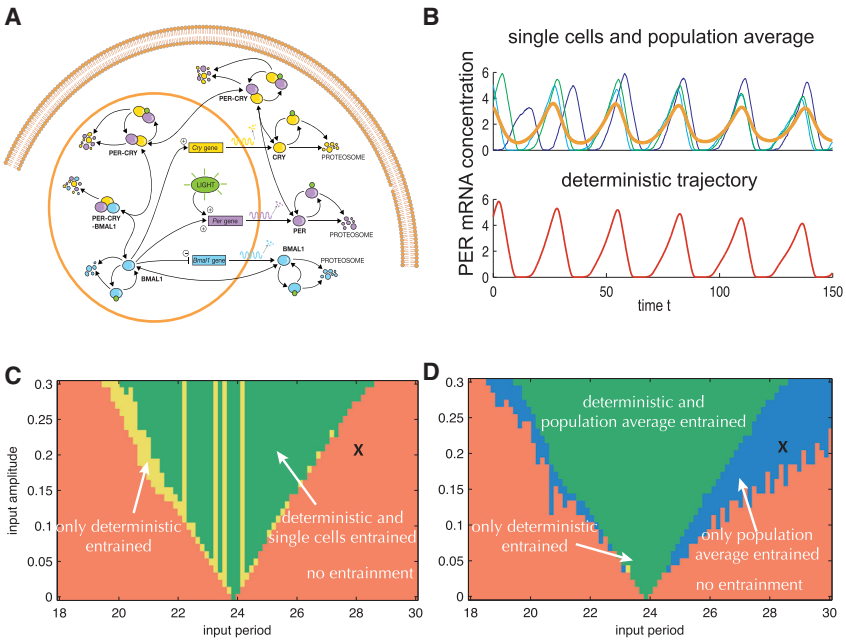

Figure 4. Stochastic Population Entrainment of the Circadian Clock Model

(A) Numerical results for the circadian clock model (Leloup and Goldbeter, 2003).

(B) Three single-cell trajectories (green, blue, and cyan), the population average of 1,000 trajectories (orange), and the corresponding deterministic trajectory are shown. The values of input frequency and amplitude used for this simulation are marked with × in the Arnol'd Tongues below. It can be seen that the single-cell trajectories are incoherent but similar in behavior to the deterministic trajectory, while the population-averaged trajectory undergoes regular oscillations with a lower amplitude and with frequency ω_f.

(C) The entrainment regions (Arnol'd Tongues) for deterministic and single-cell cases are compared. These two tongues match closely but there is a small area (yellow) where only the deterministic response entrains but the single-cell response does not.

(D) The Arnol'd Tongues for deterministic and population-level cases are compared, and one can clearly see that the population-level tongue is much broader. Specifically in the blue region, only the population-level signal entrains while the deterministic signal does not, illustrating that intrinsic noise causes the entrainment response to be more robust at the population level in comparison to both single-cell and deterministic cases. The Arnol'd Tongues are computed using 500 single-cell trajectories at each input frequency and amplitude.

steady-state distribution of $\phi_0(t)/2\pi$ ($\phi_0(t)$ modulo 2π) to be almost uniform over $[0,2\pi]$. Using this fact and the 2π-periodicity of x_0, we can show that the population-level response $\mathbb{E}(x(t))$ (where $\mathbb{E}$ denotes the expectation operator) of several noisy single-cell trajectories reduces to some constant C_0 for large values of time t:

$$\mathbb{E}(x(t)) \approx \mathbb{E}(x_0(\omega_0 t + \phi_0(t))) = \frac{1}{2\pi}\int_0^{2\pi} x_0(\omega_0 t + \phi) d\phi = \frac{1}{2\pi}\int_0^{2\pi} x_0(\phi) d\phi := C_0. \quad \text{(Equation 4)}$$

This implies that for large t, the phase variability between different single cells becomes so extreme that the oscillatory activity cancels out at the population level. Such a behavior is consistent with the existing theoretical results on noisy oscillators (Gupta et al., 2014), as well as particular computational and experimental studies on uncoupled circadian clocks with noisy dynamics (Bagheri et al., 2008; To et al., 2007; Tay et al., 2010; Ohta et al., 2005; Welsh et al., 1995; Aton et al., 2005). Note, however, that this behavior is quite unlike the noise-free system (Equation 3) where the solutions oscillate consistently with frequency ω_0.

We now consider the single-cell dynamics under a weak periodic forcing input of the form $\varepsilon u_f(\omega_f t)$, for some 2π-periodic function u_f. Here, $\varepsilon \ll 1$ is the input strength and ω_f is the forcing frequency. The dynamics of noisy single cells under this input signal can be described by a stochastic differential equation of the form Equation 1 with $F(x,t) = F_0(x) + \varepsilon u_f(\omega_f t)$. Note that due to nonlinearities in the dynamics, the dependence of the single-cell trajectories $(x(t))_{t\geq 0}$ on the periodic input can be very complicated. However, using perturbation analysis we can show that these trajectories can be viewed as the superposition of two signals: a strong signal with natural frequency ω_0 and a weak signal with forcing frequency ω_f:

$$x(t) \approx x_0(\omega_0 t + \phi_0(t)) + \varepsilon x_f(\omega_f t + \phi_f(t)), \quad \text{(Equation 5)}$$

where x_0, $\phi_0(t)$ are as before, x_f is some 2π-periodic function, and $\phi_f(t)$ is a random variable that corresponds to the phase of the forcing component.

Equation 5 forms the basis for mathematically understanding the enhancement of entrainment at the population level (that is, the stochastic population entrainment we describe above) and the role of intrinsic noise in causing this effect. In the absence of this noise, $\phi_0(t)$ and $\phi_f(t)$ become deterministic constants, and the resulting deterministic (single-cell and population-level) signal oscillates incoherently (see Figure 5A). This signal is clearly not entrained as can be seen from its power spectral density shown in Figure 5B. We explained above that in the presence of intrinsic noise, the natural phase variable $\phi_0(t)$ (modulo 2π) has a steady-state distribution that is almost uniform over the interval $[0,2\pi]$. This intrinsic noise also affects the forcing phase variable $\phi_f(t)$, but notably, this effect is strikingly different. Instead of having the phase-uniformization effect, intrinsic noise imposes on the forcing component a phase-focusing effect, which ensures that the steady-state distribution of the forcing phase variable $\phi_f(t)$ (modulo 2π) is unimodal in the sense that it is concentrated around a certain value ϕ_f^*.

Both these effects can be clearly observed for the spiky NF-κB and the circadian clock model in Figures 6A and 6B. At the single-cell level, $\phi_0(t)$ and $\phi_f(t)$ assume different values for different

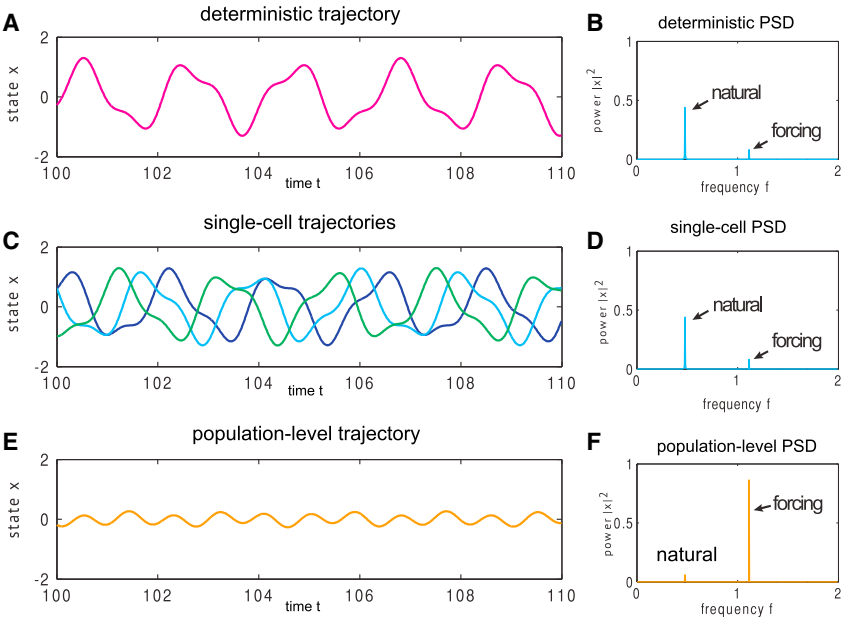

Figure 5. Understanding Stochastic Population Entrainment

(A–F) For the dynamics given by Equation 5, deterministic (A) and single-cell trajectories (C) show incoherent behavior, while the population-level average of 1,000 trajectories (E) is nicely oscillating. As expected, the normalized PSD (total power is 1) of the deterministic (B) and a single trajectory (D) show two peaks, one at the natural frequency and one at the forcing frequency. On the other hand, in the normalized PSD of the population-level average of 1,000 trajectories (F), the power in the natural frequency almost disappears and nearly all the power is concentrated at the forcing frequency. The trajectories were computed according to Equation 5 with $x_0(t) = x_f(t) = \cos(t)$, $\varepsilon = 0.3$, $\omega_0 = 3$, and $\omega_f = 7$. For the deterministic trajectory $\phi_0(t) = \phi_f(t) = 0$ and for the single-cell and population-level trajectories $\phi_0(t) \sim \mathcal{U}(0, 2\pi)$ and $\phi_f(t) \sim \mathcal{U}(0, (\pi/2))$, where $\mathcal{U}(a, b)$ denotes the uniform distribution over the interval (a,b).

See also Figure S4.

cells, resulting in variability among trajectories of Equation 5 (see Figure 5C). These trajectories oscillate incoherently as in the deterministic case and their power spectral density (see Figure 5D) confirms that they are not entrained. However, the asymmetric action of intrinsic noise on the natural and the forced components of Equation 5 results in the cancelling out of the oscillations in the natural component in Equation 5 at the population level, even though the oscillations in the forcing component still remain, thereby yielding a coherent population-level signal (see Figure 5E) that is entrained to the input signal as indicated by its power spectral density (see Figure 5F). To see this mathematically, note that the steady-state expectation of single-cell dynamics (Equation 5) can be computed as

$$\begin{aligned}\mathbb{E}(x(t)) &\approx \mathbb{E}(x_0(\omega_0 t + \phi_0(t))) + \varepsilon \mathbb{E}(x_f(\omega_f t + \phi_f(t))) \\ &= C_0 + \varepsilon \bar{x}_f(\omega_f t + \phi_f^*),\end{aligned} \qquad \text{(Equation 6)}$$

where C_0 is the same as in Equation 4, and $\bar{x}_f(\omega_f t + \phi_f^*) = \mathbb{E}(x_f(\omega_f t + \phi_f))$ is the expectation with respect to some $[0,2\pi]$-valued random variable ϕ_f whose distribution is concentrated around ϕ_f^*. Because $\bar{x}_f$ is also a 2π-periodic function, the population-level signal (Equation 6) oscillates coherently with the forcing frequency ω_f, implying that it is entrained.

The behavior of deterministic, single-cell, and population-level trajectories that we inferred using Equation 6 is in good qualitative agreement with the stochastic population entrainment we observe in our examples (see Figures 3B and 4B). We conclude that this effect results from intrinsic noise and the way it interacts with the nonlinear dynamics to generate two disparate effects: phase-uniformization and phase-focusing. Effectively, while the former tries to make the distribution of the natural phase more uniform, the latter tends to constrain the distribution of the forcing phase to be unimodal. Due to phase-uniformization, the natural oscillatory component cancels out at the population level, but thanks to phase-focusing, the forcing component is preserved, leading to a signal that is entrained to the periodic forcing input. The canceling caused by phase-uniformization cannot arise in the absence of intrinsic noise or within single cells that explains why the population-level trajectories entrain more readily than deterministic and single-cell trajectories (recall the Arnol'd Tongues in Figures 3C, 3D, 4C, and 4D). Moreover the population-level entrainment achieved this way is robust under environmental or extrinsic variability among cells or to levels of intrinsic noise within the cells (see the Method Details section of the STAR Methods and Figure S3). This latter robustness is unlike the phenomenon of stochastic resonance, as we will discuss later.

Throughout the paper, we assume that all cells in the population start from the same initial state. This assumption implies that the only source of heterogeneities among cells are the random fluctuations or intrinsic noise in their intracellular dynamics. It also ensures that in the deterministic setting, the population-level signal coincides with a single-cell signal. Clearly, this assumption of all cells having the same initial state is unrealistic from a biological standpoint, and therefore it is natural to ask if the phenomenon we report will persist if this assumption is violated. Furthermore, we must check if the proposed enhancement of population-level entrainment region can be produced by simply distributing the initial states of cells randomly, but keeping their dynamics deterministic. If population-level entrainment holds under these conditions, then it raises the possibility that the effect we discover might essentially be an outcome of averaging over heterogeneous cellular states, and intrinsic noise could simply be a mechanism for creating these heterogeneities rather than playing a dynamical role as we claim above. We investigate these issues theoretically and also computationally using simulations of the NF-κB model in the Method Details section of the STAR Methods. We randomize the initial states of cells and compare the entrainment response of population averages with both types of intracellular dynamics, deterministic and stochastic (see Figure S2). We find that in both these cases, randomizing the initial states of cells has an insignificant

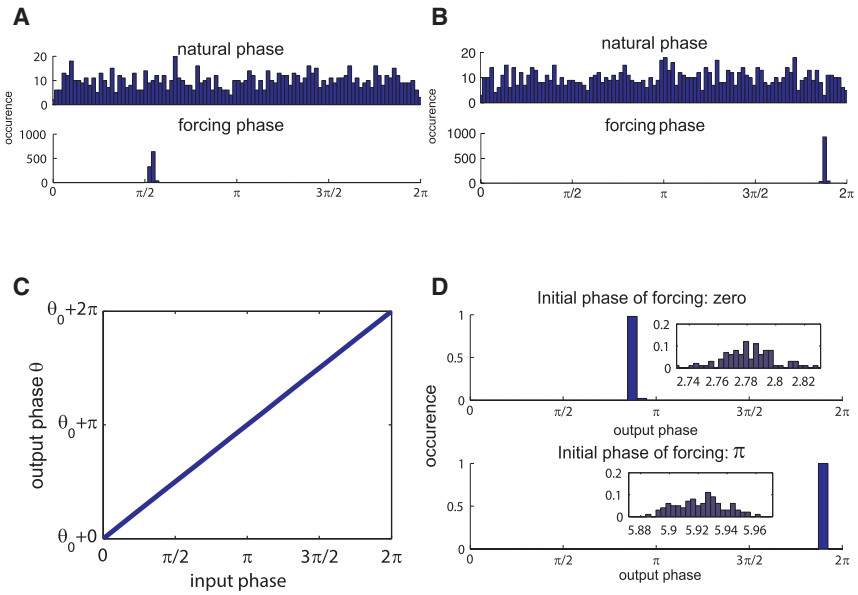

Figure 6. Phase-Distributions for the NF-κB and Circadian Clock Models

(A and B) In (A), we use 1,000 single-cell trajectories of the NF-κB model to plot the histograms exhibiting the spreadout distribution of the natural phase (ϕ_0) and the concentrated distribution of the forcing phase (ϕ_f) modulo 2π. The same is demonstrated for the circadian clock model in (B).

(C and D) Illustrations of the phase-resetting property of entrainment for the circadian clock model. Shown in (C) is the linear mapping from the input phase to the phase of the population-level signal (output phase) modulo 2π. Here, θ_0 is some constant denoting the phase shift between input and output. To demonstrate this phase resetting more clearly, in (D), we consider two input phases 0 and π and plot the phase-distribution histograms for the output phases. Both these distributions are concentrated over a narrow region (see the insets) and their means are separated by π as predicted by the linear nature of the mapping in (C).

See also Figure S4.

influence on the Arnol'd Tongues, and the entrainment region for the population average is still much wider for the stochastic case in comparison to the deterministic case. This supports our assertion that the phenomenon we describe depends critically on the dynamical nature of intrinsic noise and it cannot be replicated using static noise in the form of heterogeneous initial states.

Note that expression in Equation 5 is an approximation for single-cell oscillator dynamics that is only valid in the "weak forcing" regime. If the difference between forcing frequency ω_f and natural frequency ω_0 is large, then for regions near the boundary of Arnol'd Tongue, this expression and the ensuing analysis may not be accurate. Nevertheless, our computational results show that noise-induced entrainment still holds in these regions at the population level. It is known that in these regions the single-cell oscillators experience the "injection pulling" effect (Adler, 1946; Stover, 1966) that enables them to have oscillatory components with a variety of frequencies of the form $\omega_k = \omega_0 + k(\omega_f - \omega_0)$, for any integer k. Our computational results on the expansion of Arnol'd Tongues at the population level then suggest that in the presence of intrinsic noise, for each frequency ω_k with $k \neq 1$, the corresponding oscillatory component undergoes phase-uniformization and hence gets eliminated at the population level, while for $k = 1$, the component undergoes phase-focusing and is therefore preserved at the population level, leading to an entrained signal. Of course, this needs to be verified mathematically by deriving relations similar to Equation 5 but with additional contributions from oscillatory components with frequencies ω_k's for $k \neq 0,1$. These considerations will be explored elsewhere.

DISCUSSION

The dynamics of intracellular oscillators is generally affected by intrinsic biochemical noise, and at first glance, this noise appears to be a nuisance that may disrupt their normal functioning. Our finding in this paper indicates that exactly the opposite is true—the intrinsic noise may actually be vital in ensuring the normal functioning of oscillators in contexts where population-level behavior matters. Specifically, we show that intrinsic noise facilitates the entrainment of population-averaged response of such oscillators, a phenomenon that we call stochastic population entrainment.

There are many examples in the existing literature where noise, in various forms, can add certain desirable oscillatory characteristics to biological systems. We discuss some of these examples and indicate how stochastic population entrainment is different. We begin with the reported observation that intrinsic biochemical noise can impute oscillations to individual relaxation oscillators, which are otherwise stable in the noise-free or deterministic case (Vilar et al., 2002). In contrast, our paper considers the entrainment of so-called limit-cycle oscillators, where oscillations are sustained by the nonlinearities of the deterministic model. Indeed, the noise-induced phenomenon we present can be attributed to the interaction of these nonlinearities with intrinsic noise present within each oscillator (see The Basis of Stochastic Population Entrainment section of the Results), which is generated independently in each oscillator. This independence of noise makes our work fundamentally different both in biological context and in the mechanism of action, because in other works, a common source of noise is shared by all oscillators (Teramae and Tanaka, 2004; Jensen, 2002; Butzin et al., 2016) or the dynamics of oscillators are coupled (Zhou et al., 2002; Ullner et al., 2009).

The phenomenon of stochastic population entrainment is similar in effect to the well-known phenomenon of stochastic resonance that has been discovered in several natural and man-made systems (Gammaitoni et al., 1998; McDonnell and Abbott, 2009). In both these phenomena, dynamical noise conspires with system's nonlinearities to produce coherent oscillations at the forcing frequency. However, these phenomena are fundamentally different in their underlying mechanisms and particularly in the role of noise in creating oscillatory coherence. While stochastic resonance relies on noise reinforcing the weak

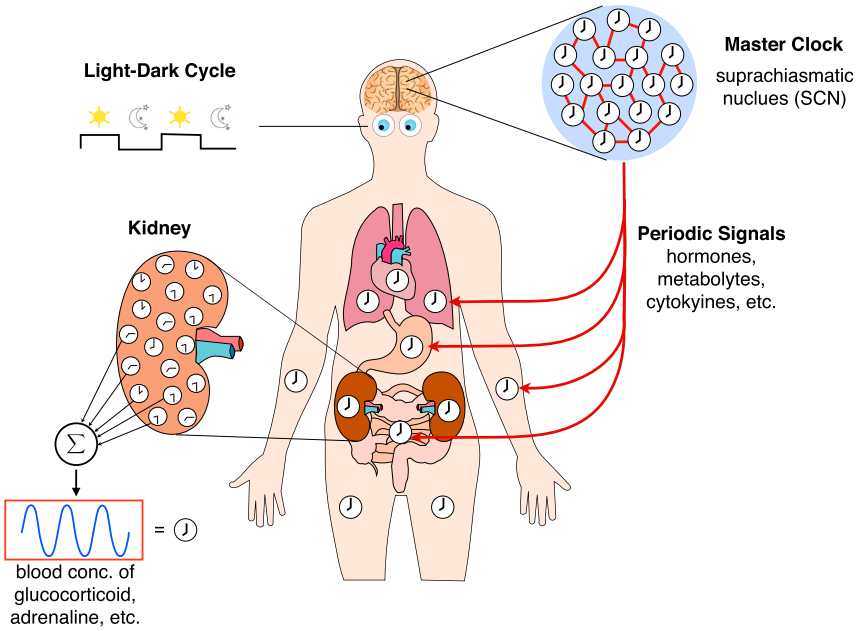

Figure 7. Schematics of the Stochastic Population Entrainment of Peripheral Clocks

This figure shows how the master clock (SCN) can reliably entrain the peripheral circadian clocks (in kidneys, liver, lungs, etc.) at the tissue level. The multicellular SCN entrains to visually observed light/dark cycles and the intercellular coupling mechanism keeps its cellular population synchronized (top right). The SCN passes periodic cues to peripheral circadian clocks that either have no coupling or weak coupling among cells. Our results indicate that even weak periodic cues are sufficient for the SCN to reliably entrain the peripheral circadian clocks at the tissue level due to Stochastic Population Entrainment, as shown here for the kidney (bottom left). Moreover, this population-level entrainment holds even though the individual circadian clocks may be out of phase with each other due to biochemical noise.

oscillatory mode of "hopping" between two stable states, stochastic population entrainment relies on noise acting differentially on the phases of the natural and the input oscillatory modes (as discussed in The Basis of Stochastic Population Entrainment section of the Results). Due to this difference in mechanisms, unlike stochastic resonance, the noise-induced phenomenon we describe is quite insensitive to the levels of noise in the system (this is demonstrated in the Method Details section of the STAR Methods).

While stochastic population entrainment is of interest in its own right as a dynamic phenomenon, its biological significance derives from the considerable importance of oscillator entrainment in biology and the critical role such entrainment plays in anticipating future physiological states and coordinating appropriate response mechanisms. In mammals, the central pacemaker SCN consists of circadian clocks that are individually sloppy and unreliable due to intrinsic noise (Welsh et al., 1995). However, the multicellular SCN exhibits remarkable time-keeping precision (Herzog et al., 2004) that persists in constant darkness (Yamazaki et al., 2000) but not in constant light (Ohta et al., 2005). Experimental (Aton et al., 2005) and computational (Bagheri et al., 2008; To et al., 2007) studies have revealed that entrainment by light/dark cycles and coupling between the individual clocks are both responsible for creating this population-level coherence in SCN from several noisy single-cell clocks. The circadian rhythms generated by SCN act as periodic cues for the peripheral circadian clocks, which are present in tissues throughout a mammalian body (Albrecht, 2012; Dibner et al., 2010; Richards and Gumz, 2012). These periodic cues are transmitted through electrical, endocrine, or metabolic signaling pathways (Albrecht, 2012; Levi and Schibler, 2007) and they cause reliable entrainment of peripheral clocks at the tissue level even though the individual peripheral clocks are considerably noisy (Balsalobre et al., 1998).

However, unlike the SCN, the peripheral circadian clocks are either uncoupled or weakly coupled, and the loss of periodic signal leads to rapid desynchronization (Nagoshi et al., 2004; Liu et al., 2007). Therefore, we cannot use the insights from SCN-based studies to understand how tissue-level (or population-level) coherence is generated and maintained by peripheral circadian clocks. Such an understanding is vital because a lack of synchrony in the circadian system is believed to lead to many diseases such as obesity, diabetes, and other psychiatric disorders (Levi and Schibler, 2007; Kalsbeek et al., 2014). Our results provide this understanding as they show that even without intercellular coupling, the peripheral circadian clocks can perfectly entrain at the tissue level to even weak periodic cues from SCN or any other source, due to stochastic population entrainment (see Figure 7). Our results also provide a possible explanation to the experimental results that show that phase differences between SCN and the peripheral tissues can be induced just by altering the feeding cycles (Damiola et al., 2000). In this case, our results suggest that the phase can be reliably set to any value (modulo 2π) simply by adjusting the phase of the input signal. This is illustrated for the circadian clock model (Leloup and Goldbeter, 2003) in Figures 6C and 6D, and this phase-resetting property is yet another interesting effect of intrinsic noise.

The circadian rhythms produced either by the SCN or the peripheral tissues can give rise to periodic cues for many intracellular oscillatory circuits. An individual oscillator may produce a noisy biochemical signal, but generally several such noisy signals get pooled at the tissue level or in the bloodstream resulting in a population-averaged signal that then drives various physiological functions. Hence, the population-level entrainment response needs to be robust, and our results provide insights on how this robustness may be achieved by a simple mechanism that utilizes intrinsic biochemical noise. As an example, consider glucose metabolism in which the production of insulin is modulated by a circadian rhythm (Boden et al., 1996), and the insulin produced by individual cells gets averaged in the bloodstream. Even though individual cells may produce noisy incoherent insulin signals, our results demonstrate that, in principle, it is possible for the population-level insulin signal to be nicely entrained to the

underlying circadian rhythm, thereby facilitating glucose homeostasis (Kalsbeek et al., 2014).

Generation of coherent tissue-level oscillations from several noisy single-cell oscillators is also important for pattern formation during embryogenesis (Oates et al., 2012). This coherence is frequently attributed to intercellular coupling, even though such coupling mechanisms have not been generally established. Our results indicate that even without this coupling, tissue-level coherence can readily emerge in the presence of a entraining periodic cue that can be weak in strength as long as it is observed by all the cells. In this sense, our results offer a fresh outlook in the study of tissue-level biological oscillations and their underlying mechanisms.

The results in this paper only apply to populations of single-cell oscillators that are dynamically uncoupled and they show that intrinsic noise can interact with the underlying nonlinear dynamics to induce entrainment of the population mean. Strictly speaking, this assumption of "no intercellular coupling" may be biologically untenable in many situations, because one is often interested in cell populations confined to a small spatial region (like a tissue), where some form of intercellular communication cannot be ruled out. In such situations, our results could still provide insights into the population-level entrainment phenomenon when the dynamic coupling is sufficiently weak on the timescale of oscillatory dynamics. For example, it is known that coupling between the circadian clock cells in SCN makes it resistant to entrainment (Abraham et al., 2010), which in turn makes the organism susceptible to jet lag when there is a phase shift in the light/dark cycles. Recent experimental results have revealed that genetic deficiencies in the coupling mechanisms or their pharmacological inhibition can enable the organism to be less prone to jet lag because their SCN can entrain more easily (Yamaguchi et al., 2013). These experimental findings are consistent with our results as they also point toward the ease of population-level entrainment of uncoupled noisy oscillators. The influence of coupling in setting the entrainment range has been studied both experimentally and theoretically (Bagheri et al., 2008; Abraham et al., 2010; Hafner et al., 2012) in the context of circadian clocks. However, in light of our results, it is evident that further analyses are required to understand how coupling mechanisms and intrinsic noise interact in setting the entrainment profiles of biological oscillators, both for single cells and the population mean. It is possible that even with coupling, intrinsic noise enables the population mean to entrain first to a periodic stimulus and then the coupling mechanisms take over to bring all the cells in unison with the population mean. This two-step process could be a reliable mechanism for synchronizing cellular populations to common periodic signals. We are pursuing these ideas in an ongoing work.

STAR★METHODS

Detailed methods are provided in the online version of this paper and include the following:

SUPPLEMENTAL INFORMATION

Supplemental Information includes four figures and two tables and can be found with this article online at http://dx.doi.org/10.1016/j.cels.2016.10.006.

AUTHOR CONTRIBUTIONS

Initial Conception: M.K.; Methodology: A.G. and M.K.; Computer Simulations: B.H. and A.G.; Software: B.H.; Analytical Derivations: A.G.; Analysis of Results: A.G., M.K., and B.H.; Writing: A.G., M.K., and B.H.; Supervision and Funding: M.K.

ACKNOWLEDGMENTS

We would like to thank Prof. Savas Tay (University of Chicago) for providing the data for Figure 1.

Received: February 15, 2016
Revised: July 4, 2016
Accepted: October 7, 2016
Published: November 3, 2016

REFERENCES

Abraham, U., Granada, A.E., Westermark, P.O., Heine, M., Kramer, A., and Herzel, H. (2010). Coupling governs entrainment range of circadian clocks. Mol. Syst. Biol. *6*, 438.

Adler, R. (1946). A study of locking phenomena in oscillators. Proc. IRE *34*, 351–357.

Albrecht, U. (2012). Timing to perfection: the biology of central and peripheral circadian clocks. Neuron *74*, 246–260.

Aton, S.J., Colwell, C.S., Harmar, A.J., Waschek, J., and Herzog, E.D. (2005). Vasoactive intestinal polypeptide mediates circadian rhythmicity and synchrony in mammalian clock neurons. Nat. Neurosci. *8*, 476–483.

Aulehla, A., and Pourquié, O. (2008). Oscillating signaling pathways during embryonic development. Curr. Opin. Cell Biol. *20*, 632–637.

Bagheri, N., Taylor, S.R., Meeker, K., Petzold, L.R., and Doyle, F.J., 3rd (2008). Synchrony and entrainment properties of robust circadian oscillators. J. R. Soc. Interface *5* (*Suppl 1*), S17–S28.

Baker, T.A., Grossman, A.D., and Gross, C.A. (1984). A gene regulating the heat shock response in escherichia coli also affects proteolysis. Proc. Natl. Acad. Sci. USA *81*, 6779–6783.

Balsalobre, A., Damiola, F., and Schibler, U. (1998). A serum shock induces circadian gene expression in mammalian tissue culture cells. Cell *93*, 929–937.

Batchelor, E., Mock, C.S., Bhan, I., Loewer, A., and Lahav, G. (2008). Recurrent initiation: a mechanism for triggering p53 pulses in response to DNA damage. Mol. Cell *30*, 277–289.

Boden, G., Ruiz, J., Urbain, J.L., and Chen, X. (1996). Evidence for a circadian rhythm of insulin secretion. Am. J. Physiol. *271*, E246–E252.

Brown, S.A., Zumbrunn, G., Fleury-Olela, F., Preitner, N., and Schibler, U. (2002). Rhythms of mammalian body temperature can sustain peripheral circadian clocks. Curr. Biol. *12*, 1574–1583.

Butzin, N.C., Hochendoner, P., Ogle, C.T., Hill, P., and Mather, W.H. (2016). Marching along to an offbeat drum: Entrainment of synthetic gene oscillators by a noisy stimulus. ACS Synth. Biol. *5*, 146–153.

Cartwright, J.H.E., Eguíluz, V.M., Hernández-García, E., and Piro, O. (1999). Dynamics of elastic excitable media. Int. J. Bifurcat. Chaos *9*, 2197–2202.

Cohen-Saidon, C., Cohen, A.A., Sigal, A., Liron, Y., and Alon, U. (2009). Dynamics and variability of ERK2 response to EGF in individual living cells. Mol. Cell *36*, 885–893.

Cooley, J.W., and Tukey, J.W. (1965). An algorithm for the machine calculation of complex Fourier series. Math. Comput. *19*, 297–301.

Damiola, F., Le Minh, N., Preitner, N., Kornmann, B., Fleury-Olela, F., and Schibler, U. (2000). Restricted feeding uncouples circadian oscillators in peripheral tissues from the central pacemaker in the suprachiasmatic nucleus. Genes Dev. *14*, 2950–2961.

Dibner, C., Schibler, U., and Albrecht, U. (2010). The mammalian circadian timing system: organization and coordination of central and peripheral clocks. Annu. Rev. Physiol. *72*, 517–549.

Dolmetsch, R.E., Xu, K., and Lewis, R.S. (1998). Calcium oscillations increase the efficiency and specificity of gene expression. Nature *392*, 933–936.

Elowitz, M.B., Levine, A.J., Siggia, E.D., and Swain, P.S. (2002). Stochastic gene expression in a single cell. Science *297*, 1183–1186.

Fitzhugh, R. (1961). Impulses and physiological states in theoretical models of nerve membrane. Biophys. J. *1*, 445–466.

Gammaitoni, L., Hänggi, P., Jung, P., and Marchesoni, F. (1998). Stochastic resonance. Rev. Mod. Phys. *70*, 223–287.

Gillespie, D.T. (1977). Exact stochastic simulation of coupled chemical reactions. J. Phys. Chem. *81*, 2340–2361.

Gillespie, D.T. (2000). Chemical Langevin equation. J. Chem. Phys. *113*, 297–306.

Gupta, A., Briat, C., and Khammash, M. (2014). A scalable computational framework for establishing long-term behavior of stochastic reaction networks. PLoS Comput. Biol. *10*, e1003669.

Hafner, M., Koeppl, H., and Gonze, D. (2012). Effect of network architecture on synchronization and entrainment properties of the circadian oscillations in the suprachiasmatic nucleus. PLoS Comput. Biol. *8*, e1002419.

Han, Q., Bagheri, N., Bradshaw, E.M., Hafler, D.A., Lauffenburger, D.A., and Love, J.C. (2012). Polyfunctional responses by human T cells result from sequential release of cytokines. Proc. Natl. Acad. Sci. USA *109*, 1607–1612.

Hayot, F., and Jayaprakash, C. (2006). NF-kappaB oscillations and cell-to-cell variability. J. Theor. Biol. *240*, 583–591.

Herzog, E.D., Aton, S.J., Numano, R., Sakaki, Y., and Tei, H. (2004). Temporal precision in the mammalian circadian system: a reliable clock from less reliable neurons. J. Biol. Rhythms *19*, 35–46.

Jensen, R.V. (2002). Synchronization of driven nonlinear oscillators. Am. J. Phys. *70*, 607.

Jensen, M.H., and Krishna, S. (2012). Inducing phase-locking and chaos in cellular oscillators by modulating the driving stimuli. FEBS Lett. *586*, 1664–1668.

Kalsbeek, A., la Fleur, S., and Fliers, E. (2014). Circadian control of glucose metabolism. Mol. Metab. *3*, 372–383.

Kanamaru, T. (2007). Van der Pol oscillator. Scholarpedia *2*, 2202.

Keener, J.P., and Sneyd, J. (2005). A Mathematical Textbook of Physiology, Second Edition (Springer-Verlag).

Kellogg, R.A., and Tay, S. (2015). Noise facilitates transcriptional control under dynamic inputs. Cell *160*, 381–392.

Kloeden, P.E., and Platen, E. (1992). Numerical Solution of Stochastic Differential Equations (Springer-Verlag), pp. 1–7.

Krishna, S., Jensen, M.H., and Sneppen, K. (2006). Minimal model of spiky oscillations in NF-kappaB signaling. Proc. Natl. Acad. Sci. USA *103*, 10840–10845.

Kurtz, T.G. (1978). Strong approximation theorems for density dependent Markov chains. Stochastic Process. Appl. *6*, 223–240.

Leloup, J.-C., and Goldbeter, A. (2003). Toward a detailed computational model for the mammalian circadian clock. Proc. Natl. Acad. Sci. USA *100*, 7051–7056.

Levi, F., and Schibler, U. (2007). Circadian rhythms: mechanisms and therapeutic implications. Annu. Rev. Pharmacol. Toxicol. *47*, 593–628.

Lin, Y., Sohn, C.H., Dalal, C.K., Cai, L., and Elowitz, M.B. (2015). Combinatorial gene regulation by modulation of relative pulse timing. Nature *527*, 54–58.

Liu, A.C., Welsh, D.K., Ko, C.H., Tran, H.G., Zhang, E.E., Priest, A.A., Buhr, E.D., Singer, O., Meeker, K., Verma, I.M., et al. (2007). Intercellular coupling confers robustness against mutations in the SCN circadian clock network. Cell *129*, 605–616.

McDonnell, M.D., and Abbott, D. (2009). What is stochastic resonance? Definitions, misconceptions, debates, and its relevance to biology. PLoS Comput. Biol. *5*, e1000348.

Mitarai, N., Alon, U., and Jensen, M.H. (2013). Entrainment of noise-induced and limit cycle oscillators under weak noise. Chaos *23*, 023125.

Nagoshi, E., Saini, C., Bauer, C., Laroche, T., Naef, F., and Schibler, U. (2004). Circadian gene expression in individual fibroblasts: cell-autonomous and self-sustained oscillators pass time to daughter cells. Cell *119*, 693–705.

Oates, A.C., Morelli, L.G., and Ares, S. (2012). Patterning embryos with oscillations: structure, function and dynamics of the vertebrate segmentation clock. Development *139*, 625–639.

Ohta, H., Yamazaki, S., and McMahon, D.G. (2005). Constant light desynchronizes mammalian clock neurons. Nat. Neurosci. *8*, 267–269.

Øksendal, B. (2003). Stochastic Differential Equations, Universitext, Sixth Edition (Springer-Verlag).

Pikovsky, A., Rosenblum, M., and Kurths, J. (2000). Phase synchronization in regular and chaotic systems. Int. J. Bifurcat. Chaos *10*, 2291–2305.

Pikovsky, A., Rosenblum, M., and Kurths, J. (2001). Synchronization: A Universal Concept in Nonlinear Sciences (Cambridge University Press).

Purvis, J.E., and Lahav, G. (2013). Encoding and decoding cellular information through signaling dynamics. Cell *152*, 945–956.

Reppert, S.M., and Weaver, D.R. (2002). Coordination of circadian timing in mammals. Nature *418*, 935–941.

Richards, J., and Gumz, M.L. (2012). Advances in understanding the peripheral circadian clocks. FASEB J. *26*, 3602–3613.

Stover, H.L. (1966). Theoretical explanation for the output spectra of unlocked driven oscillators. Proc. IEEE *54*, 310–311.

Tay, S., Hughey, J.J., Lee, T.K., Lipniacki, T., Quake, S.R., and Covert, M.W. (2010). Single-cell NF-kappaB dynamics reveal digital activation and analogue information processing. Nature *466*, 267–271.

Teramae, J.N., and Tanaka, D. (2004). Robustness of the noise-induced phase synchronization in a general class of limit cycle oscillators. Phys. Rev. Lett. *93*, 204103.

To, T.-L., Henson, M.A., Herzog, E.D., and Doyle, F.J., 3rd (2007). A molecular model for intercellular synchronization in the mammalian circadian clock. Biophys. J. *92*, 3792–3803.

Ullner, E., Buceta, J., Díez-Noguera, A., and García-Ojalvo, J. (2009). Noise-induced coherence in multicellular circadian clocks. Biophys. J. *96*, 3573–3581.

van der Pol, B. (1926). Lxxxviii. on "relaxation-oscillations". Lond. Edinb. Dubl.Phil. Mag. *2*, 978–992.

Vicker, M.G. (2002). Eukaryotic cell locomotion depends on the propagation of self-organized reaction-diffusion waves and oscillations of actin filament assembly. Exp. Cell Res. *275*, 54–66.

Vilar, J.M.G., Kueh, H.Y., Barkai, N., and Leibler, S. (2002). Mechanisms of noise-resistance in genetic oscillators. Proc. Natl. Acad. Sci. USA *99*, 5988–5992.

Welsh, D.K., Logothetis, D.E., Meister, M., and Reppert, S.M. (1995). Individual neurons dissociated from rat suprachiasmatic nucleus express independently phased circadian firing rhythms. Neuron *14*, 697–706.

Yamaguchi, Y., Suzuki, T., Mizoro, Y., Kori, H., Okada, K., Chen, Y., Fustin, J.-M., Yamazaki, F., Mizuguchi, N., Zhang, J., et al. (2013). Mice genetically deficient in vasopressin V1a and V1b receptors are resistant to jet lag. Science *342*, 85–90.

Yamazaki, S., Numano, R., Abe, M., Hida, A., Takahashi, R., Ueda, M., Block, G.D., Sakaki, Y., Menaker, M., and Tei, H. (2000). Resetting central and peripheral circadian oscillators in transgenic rats. Science *288*, 682–685.

Zhou, C., Kurths, J., Kiss, I.Z., and Hudson, J.L. (2002). Noise-enhanced phase synchronization of chaotic oscillators. Phys. Rev. Lett. *89*, 014101.

STAR★METHODS

KEY RESOURCES TABLE

REAGENT or RESOURCE	SOURCE	IDENTIFIER
Software and Algorithms		
Stochastic Simulation Algorithm	Gillespie, 1977	N/A
Langevin Approximation	Gillespie, 2000	N/A
Fast Fourier Transform (FFT)	Cooley and Tukey, 1965	N/A
Euler-Maruyama Scheme	Kloeden and Platen, 1992	N/A
Other		
Data for Figure 1	Kellogg and Tay, 2015	N/A

CONTACT FOR REAGENT AND RESOURCE SHARING

As Lead Contact, Prof. Mustafa Khammash is responsible for all reagent and resource requests. Please contact Prof. Mustafa Khammash at mustafa.khammash@bsse.ethz.ch with requests and inquiries.

METHOD DETAILS

We used computational models for studying the dynamics of various oscillators. All the oscillators were represented as reaction networks. In the noise-free (deterministic) setting the oscillatory trajectory of a single-cell is simulated by representing the reaction dynamics as an ordinary differential equation (ODE). In the stochastic setting, this dynamics is modeled as a continuous time Markov chain, and it is either simulated exactly using Gillespie's Stochastic Simulation Algorithm (Gillespie, 1977) or its Langevin approximation (Gillespie, 2000) is derived and the resulting Stochastic Differential Equation (SDE) is simulated. Below we provide more details on the reaction network models and their simulations.

Model Descriptions

In the paper we consider two examples of biological oscillators: the circadian clock model (Leloup and Goldbeter, 2003) and the Spiky NF-κB model (Krishna et al., 2006). Additionally, we also study the classical Van der Pol oscillator (van der Pol, 1926; Kanamaru, 2007; Mitarai et al., 2013) which is used to model many physical and biological processes (Cartwright et al., 1999; FitzHugh, 1961).

Each oscillator can be modeled as a reaction network with d species and M reactions. In the deterministic (noise-free) setting, the dynamics can be simulated by solving the ODE given by the Reaction Rate Equation (RRE) for the reaction network. In the stochastic setting we either simulate the exact copy-number dynamics using Gillespie's *Stochastic Simulation Algorithm*(SSA) (Gillespie, 1977) or we assume that the copy-numbers of all the species are large enough to ensure that the random effects are *weak* and the dynamics can be well-approximated by an appropriately formulated Langevin equation (Gillespie, 2000; Kurtz 1978). This assumption is made to make the subsequent analysis more computationally tractable, as it allows us to express the dynamics as a *stochastic differential equation* (SDE) (Øksendal, 2003) which is easier to simulate. This SDE has the form

$$dX_t = \mu(X_t, t)dt + \frac{1}{\sqrt{\Omega}}\sigma(X_t, t)dW(t) \tag{1}$$

where $X_t \in \mathbb{R}^d$ is the state vector representing the species *concentrations* at time t, $\mu(X_t, t) \in \mathbb{R}^d$ is the time-dependent drift term, $\sigma(X_t, t)$ is the time-dependent diffusion matrix of size $d \times M$, $W(t) = (W_1(t), \ldots, W_M(t))$ is the standard Brownian motion in $\mathbb{R}^M$ and Ω is the system-size or volume parameter. Suppose that when $X_t = x$, the *flux* of the k-th reaction at time t is $\lambda_k(x, t)$ and this reaction displaces the state by the *stoichiometry vector* s_k. Then the Langevin SDE has the form (1) with

$$\mu(X_t, t) = \sum_{k=1}^{M} \lambda_k(X_t, t)s_k \tag{2}$$

and $\sigma(X_t, t)$ being the $d \times K$ matrix with columns $\sigma_1(X_t, t), \ldots, \sigma_M(X_t, t)$ where

$$\sigma_k(X_t, t) = \sqrt{\lambda_k(X_t, t)}s_k, \tag{3}$$

for each $k = 1, \ldots, M$.

In this paper we solve the above SDE using the Euler-Maruyama scheme (Kloeden and Platen, 1992). Note that we can *turn-down* the level of intrinsic noise by increasing Ω. In particular if we set Ω to be ∞, then the intrinsic noise is completely *switched-off* and we recover the RRE corresponding to the deterministic model

$$\frac{dX_t}{dt} = \mu(X_t, t). \tag{4}$$

This is consistent with the dynamical law of large numbers for stochastic models of reaction networks (Kurtz, 1978).

Note that each stochastic trajectory can be viewed as the dynamics of a single oscillator (or a single cell) in the presence of intrinsic noise. By pooling together several such trajectories and taking their average (at each time-point) we obtain a signal which corresponds to the *population-level response* of an ensemble of oscillators (or single cells) in the presence of intrinsic noise. If intrinsic noise is absent then the response of each oscillator is identical to the trajectory obtained by simulating the RRE (Equation 4) for the deterministic model.

In each of the examples, we consider the oscillatory dynamics under a forcing mechanism of the form:

$$u(t) = u_0 + A\sin(\omega_f t), \tag{5}$$

where u_0 is the forcing offset, A is the forcing amplitude and ω_f is the frequency of the forcing in *radians/time unit*. We now provide more computational details for each of the examples.

Van der Pol oscillator:

The Van der Pol Oscillator consists of two species $\boldsymbol{S}_1$, $\boldsymbol{S}_2$ and four reactions, which are given by

k	Reaction	$\lambda_k(x,t)$
1	$\varnothing \rightarrow S_1$	$\lvert x_2 \rvert$
2	$S_2 \rightarrow \varnothing$	$\lvert Bx_1^2 \rvert x_2$
3	$\varnothing \rightarrow S_2$	$\lvert u(t) + dx_2 \rvert$
4	$S_2 \rightarrow \varnothing$	$\lvert x_1 \rvert$

where $B = 10$, $d = 2$ and x_i is the concentration of species S_i for $i = 1, 2$. Here $u(t)$ is the periodic forcing of the form (5) with $u_0 = 0$. The natural frequency of the system is $\omega_0 \simeq 2\pi \times 0.1065$. The concentration x_1 of species S_1 is considered to be the output of the system.

For this reaction network, the drift vector $\mu(x,t)$ and the diffusion matrix $\sigma(x,t)$ are given by

$$\mu(x,t) = \begin{pmatrix} u(t) + (d - \overset{x_2}{B}x_1^2)x_2 - x_1 \end{pmatrix}$$

and

$$\sigma(x,t) = \begin{pmatrix} \sqrt{\lvert x_2 \rvert} & 0 & 0 & 0 \\ 0 & \sqrt{\lvert Bx_1^2 x_2 \rvert} & \sqrt{\lvert u(t) + d \cdot x_2 \rvert} & \sqrt{\lvert x_1 \rvert} \end{pmatrix}$$

respectively. We set the volume to be $\Omega = 5 \cdot 10^3$ and simulate the stochastic dynamics by solving the SDE (1) with initial state $X_0 = (1, 1)$. This SDE is solved until time $t_f = 10000$ using the Euler-Maruyama scheme with step-size $dt = 0.1$.

Circadian Clock Model

The circadian clock model (Leloup and Goldbeter, 2003) is a large reaction network consisting of 16 species and 52 reactions. We use the stochastic formulation given in (To et al., 2007) and simulate the stochastic dynamics of the species copy-numbers using Gillespie's SSA (Gillespie, 1977). The forcing signal of the form (5) (with $\boldsymbol{u}_0 = 1$) enters as a multiplicative modulation of the PER mRNA transcription rate. The output we track in this example is the molar concentration of PER mRNA. This concentration is obtained by dividing the copy-number of the PER mRNA by the scaling factor $\boldsymbol{\Omega} = 600$ which corresponds to a volume of $\boldsymbol{V} = 1.7\boldsymbol{e}^{-15}$ ***liters*** as discussed in the supplementary material of (To et al., 2007). Without the periodic forcing, the natural frequency of this output is $\omega_0 = 2\boldsymbol{\pi}/23.8607$ ***radians/hrs***.

Spiky NF-κB Model

The Spiky NF-κB model we consider is based on the deterministic model by Krishna et al. (Krishna et al., 2006) and it consists of three species $\boldsymbol{N_n}$, $\boldsymbol{I_m}$, $\boldsymbol{I}$ and five reactions, given by

k	Reaction	$\lambda(t,x)$
1	$\varnothing \rightarrow N_n$	$A\frac{1-x_1}{\varepsilon+x_3}$
2	$N_n \rightarrow \varnothing$	$B\frac{x_1x_3}{\delta+x_1}$
3	$\varnothing \rightarrow I_m$	x_1^2
4	$I_m \rightarrow I$	x_2
5	$I \rightarrow \varnothing$	$C_0u(t)\frac{(1-x_1)x_3}{\varepsilon+x_3}$

where $x=(x_1,x_2,x_3)$ is the vector of concentrations of species in the following order N_n, I_m, I. The values of various parameters are $A=0.007, B=954.5, C_0=0.035, \varepsilon=2\cdot10^{-5}$ and $\delta=0.029$.

For this reaction network, the drift vector $\mu(x,t)$ is

$$\mu(x,t)=\begin{pmatrix} A\dfrac{(1-x_1)}{\varepsilon+x_3}-B\dfrac{(x_1x_3)}{\delta+x_1} \\ x_1^2-x_2 \\ x_2-u(t)x_3\dfrac{(1-x_1)}{\varepsilon+x_3} \end{pmatrix},$$

where $u(t)$ is the forcing function of the form (5) with $u_0=1$. The 3×5 diffusion matrix $\sigma(x,t)$ is given by

$$\sigma(x,t)=\begin{pmatrix} \sqrt{A\dfrac{(1-x_1)}{\varepsilon+x_3}} & \sqrt{B\dfrac{(x_1x_3)}{\delta+x_1}} & 0 & 0 & 0 \\ 0 & 0 & \sqrt{x_1^2} & -\sqrt{x_2} & 0 \\ 0 & 0 & 0 & +\sqrt{x_2} & \sqrt{u(t)x_3\dfrac{(1-x_1)}{\varepsilon+x_3}} \end{pmatrix}.$$

In the stochastic setting we set the volume to be $\Omega=N_A\cdot10^{-11}\simeq6.02\cdot10^{12}$ where N_A is the Avogadro constant. We simulate the stochastic dynamics by solving the SDE (1) with initial state $X_0=(0,0,0)$. This SDE is solved until time $t_f=1000$ using the Euler-Maruyama scheme with step-size $dt=10^{-4}$. Note that the negative states are set to zero after each integration step, to ensure that the states of the system are non-negative. The output we track is the concentration of species N_n. Without the periodic forcing, the natural frequency of this output is $\omega_0\simeq 2\pi/2.1$ *radians/hrs*.

Entrainment of van der Pol Oscillators

We consider the Van der Pol model given in (Mitarai et al., 2013) with a forcing mechanism of the form (5) with $u_0=0$. In Figure S1A we plot three single-cell trajectories in the presence of intrinsic noise and the population-level trajectory obtained by averaging 1000 single-cell trajectories. In Figure S1B we plot the trajectory in the deterministic (noise-free) case. One can observe that the stochastic single-cell trajectories have an oscillatory behavior similar to the deterministic trajectory. However, the intrinsic noise induces phase-diffusion which makes single-cell signals less coherent. These effects are averaged out at the population-level and well-behaved dynamics emerges, which is better entrained to the input signal.

Let ϕ_0 (ϕ_f) denote the phase for the natural (forcing) component in the output signal. We argued in the main paper that population-level coherence arises because at large times, the distribution of $\phi_0/2\pi$ (ϕ_0 modulo 2π) is almost uniform while the distribution of $\phi_f/2\pi$ is concentrated around a certain value. We confirm that this is indeed true by plotting the histograms for $\phi_0/2\pi$ and $\phi_f/2\pi$ in Figure S1C.

In Figure S1D and S1E, we compare the Arnol'd Tongues for the single-cell and population-level cases with the deterministic case. In comparison to the deterministic case, the total area of the entrainment region shrinks by less than 1% for the single-cell case, but it expands by more than 40% for the population-level case. This supports our main finding in the paper that intrinsic noise enables a more robust entrainment response at the population-level even though it may harm the entrainment response at the single-cell level.

To see whether the percentages we compute for the shrinkage or expansion of the Arnol'd Tongues are *robust* with respect to perturbations in the model parameters we performed a sensitivity check for these percentages. We perturbed the model parameters B and d by $\pm10\%$ of their original values ($B=10$ and $d=2$), one at a time, and computed these percentages in each case. The results are reported in Table S1 and they show that the effect we describe is quite robust with respect to the model parameters.

In Figure S1 we also provide the *color-code* used in the paper for differentiating various regions in the Arnol'd Tongues based on whether the different types of signals (single-cell, population-level or deterministic) entrain or not.

Effects of Extrinsic Noise

Throughout the paper we only consider *intrinsic* noise, that arises due to the random nature of intracellular interactions, and we do not consider *extrinsic* noise which captures the variability in the environments of different cells. The reason for this exclusion is because

the phenomenon we describe and analyze is solely due to intrinsic noise. Indeed, there is nothing deep or profound about the role of extrinsic noise in entrainment, and adding it would simply obfuscate the truly subtle interactions of intrinsic noise with dynamics, which is the focus of our paper. To support our point, we next argue that extrinsic noise *cannot destroy* the intrinsic noise-induced entrainment at the population-level reported here.

Extrinsic noise may be modeled by endowing each cell with its own private parameters θ drawn from a certain probability distribution Θ that describes the extrinsic variability of the population. Suppose that when both intrinsic and extrinsic noise are present, the dynamics of a single-cell is given by $x_\theta(t)$. Note that in this case, the population-averaged dynamics can be written as

$$\overline{x}(t) = \mathbb{E}(x_\theta(t)) = \mathbb{E}_\Theta(\mathbb{E}(x_\theta(t) \mid \theta)), \tag{6}$$

where $\mathbb{E}_\Theta$ is the expectation over the distribution of the random variable θ, and $\mathbb{E}(\bullet \mid \theta)$ is the conditional expectation given a realization of θ. Formula (6) states that the average or expectation $(\mathbb{E})$ over the whole population can be broken down into two parts - the first part $\mathbb{E}(\bullet \mid \theta)$ is the expectation over the *intrinsic noise* for a given realization of the cell's parameters θ, while the second part $\mathbb{E}_\Theta$ is the expectation over the *extrinsic noise* represented by the probability distribution Θ of θ.

Our results disregard extrinsic noise and show that for any fixed value θ, the population-averaged dynamics $y_\theta(t) = \mathbb{E}(x_\theta(t)|\theta)$ has more robust entrainment response than the single-cell dynamics $x_\theta(t)$ due to the intrinsic noise. This automatically implies that when extrinsic noise is also considered, the population-averaged dynamics $\overline{x}(t)$ given by (6) will also have more robust entrainment response than the single-cell dynamics $x_\theta(t)$. This is because if $y_\theta(t)$ oscillates with input frequency ω_f then $\overline{x}(t)$ will also oscillate with input frequency ω_f. To see this note that for $T_p = 2\pi/\omega_f$ and any $t \geq 0$, if we have $y_\theta(t+T_p) = y_\theta(t)$, then we will also have $\overline{x}(t+T_p) = \mathbb{E}_\Theta(y_\theta(t+T_p)) = \mathbb{E}_\Theta(y_\theta(t)) = \overline{x}(t)$.

The above discussion suggests that extrinsic noise adds another layer of averaging $(\mathbb{E}_\Theta)$ which *does not harm entrainment at the population-level*. In fact, extrinsic noise may even *improve entrainment* at the population-level, as it is indeed possible for several *unentrained* signals to produce an *entrained* signal on average, just like the effect described in this paper. Even though extrinsic noise may accentuate our reported noise induced entrainment (in some cases), we did not consider it in this paper because it may mask the effect of intrinsic noise which is the real cause of entrainment of the population-average. Moreover enhancing entrainment by adding extrinsic noise, would neither be fair nor biologically interesting, as it will depend crucially on a careful selection of parameter distribution, which is hard to achieve by "real" systems.

Finally we would like to mention that unlike the population-level, it is hard to judge whether extrinsic noise hinders or helps entrainment at the single-cell (or individual) level. Extrinsic noise can improve or hinder entrainment of single-cells simply by randomly selecting parameters that support or inhibit entrainment at any given forcing frequency and amplitude. These effects are rather trivial in nature and inconsequential for the phenomenon we report here.

Effects of Randomizing the Initial States

In this paper we assume that all the cells have the same initial state, and so cell-to-cell heterogeneities only arise due to random fluctuations or intrinsic noise in the intracellular dynamics. This assumption will almost never be satisfied by biological cells and hence it is natural to ask if the effect we describe will persist if these initial states are randomly distributed. More importantly one may wonder if such a random distribution of initial states is *alone sufficient* to create the effect we describe, without the need of dynamical intrinsic noise. If this happens then it will raise concerns that perhaps randomization of cellular states is responsible for the enhancement of entrainment region at the population-level, and the dynamical nature of noise is not important for this effect, contrary to the claim of this paper. We can check this by comparing the entrainment response of a population of cells with randomized initial states, with (stochastic) or without (deterministic) intrinsic noise in the intracellular dynamics. We find that randomizing the initial states has an *insignificant influence* on the entrainment regions in both these cases (stochastic and deterministic). Therefore the phenomenon we report is also relatively unaffected by this randomization of initial states, reinforcing our claim that the dynamical nature of noise is really important for this phenomenon.

We show this computationally for the Spiky NF-κ B model described before. Earlier we had set the initial states of the cells to be $x_0 = (0, 0, 0)$. We compare this case of constant initial conditions to the situation where the initial state of each cell is randomly and independently chosen from the uniform distribution over the unit cube $[0, 1]^3$. Since each cell has its own initial condition, the population-level signal will differ from the single-cell signal even in the deterministic case. We compare the Arnol'd Tongues in these two scenarios (constant and randomly distributed initial states) for the population-level signal with deterministic intracellular dynamics in Figure S2A. The same comparison is made for the stochastic dynamics in Figure S2B. Note that irrespective of the nature of dynamics, randomizing the initial states does not change the Arnol'd Tongues significantly. Consequently the Arnol'd Tongue for the population-level entrainment response are still much wider in the stochastic case in comparison to the deterministic case, even when we randomize the initial states (see Figure S2D). The enhancement effect is quite similar to the constant initial-states scenario presented in the main paper and also displayed in Figure S2C for convenience. We can quantify this enhancement effect by computing the percentage of expansion of the Arnol'd Tongue area in the stochastic case in comparison to the deterministic case. These percentages are 54% and 59% for the constant initial-states and the random initial-states situations respectively, again indicating that the overall enhancement effects are quite similar. However it is noteworthy that this effect is *slightly more* when the initial states are randomized. These numerical experiments with the NF-κ B model clearly show that static noise, in the form of randomized initial states, is not responsible for the phenomenon we report and dynamical noise is necessary to see the proposed effect. In the case of weak forcing, this insight can also be obtained from the mathematical analysis we present later for a simple example.

The paragraph after Equation (35) discusses why randomness in the dynamics plays a unique role in causing population-level entrainment and also explains why this role cannot be performed by randomness in the initial states.

Effects of Altering the Noise-Levels

We mentioned in the main paper that the phenomenon we describe is similar to the well-known phenomenon of *stochastic resonance* (Gammaitoni et al., 1998; McDonnell and Abbott, 2009), where also dynamical noise interacts with system's nonlinearities to create coherent oscillations at the forcing frequency. However there is a mechanistic difference between these two phenomena which manifests in the role of noise in creating oscillatory coherence. In *stochastic resonance*, noise reinforces the *weak* oscillatory mode of "hopping" between two stable states, and hence this phenomenon depends critically on the level of noise in the system. On the other hand, the phenomenon we report relies on noise having contrasting effects on the phase-distribution of the natural and the input oscillatory modes (see the Mathematical Explanation section). As these effects are robust to noise-levels, the same is true for the reported noise-induced entrainment phenomenon, quite unlike the phenomenon of *stochastic resonance*.

We demonstrate this using simulations of the Spiky NF-κ B model. In earlier simulations we had set the cell-volume to be $\Omega = N_A \times 10^{-11}$, where N_A is the Avogadro's constant. Since we simulate the dynamics using Langevin SDE (1), the noise-level in the dynamics is proportional to $1/\sqrt{\Omega}$. Hence we can alter the noise-levels by varying the cell-volume Ω and observe the effect on the population-level Arnol'd Tongues in the stochastic setting. We compare these Arnol'd Tongues with the deterministic Arnol'd Tongues for six different volume parameters in Figure S3, and we find that these six cases are very similar to each other. We can quantify the population-level entrainment enhancement effect by computing the percentage of expansion of the Arnol'd Tongue area in the stochastic case in comparison to the deterministic case. These percentages, reported in Table S2 for the six different volume parameters, again show that the effect is quite similar for the six cases. From these numerical experiments we can conclude that the phenomenon we describe is quite robust to the noise-levels in the dynamics. However note that the amplitude of the population-level oscillatory signal and the cut-off times needed to reach steady-state may depend on the noise-level, as indicated by the analysis in the Mathematical Explanation section for a simple example.

Mathematical Explanation

In this section we mathematically explain the noise-induced entrainment phenomenon using a simple example. We model the dynamics of a single cell (or a single oscillator) kept under constant environmental conditions, by a two-dimensional self-sustained oscillator whose stable limit cycle is a perfect circle centered at the origin. We add *noise* or *randomness* into the dynamics and discuss its effects on the oscillations at both the single-cell and the population level. We then introduce periodic forcing, with a *weak* strength, to the single-cell dynamics and again analyze the oscillatory activity at both the single-cell and the population level results show that the weak forcing is able to entrain the dynamics at the population level but not at the single-cell level. Moreover this behavior only holds in the presence of noise and hence the corresponding deterministic system will not get entrained by the weak input. These observations demonstrate the main findings of the paper.

Self-Sustained Oscillators

Suppose that the dynamics of a single cell with constant environmental conditions and without any noise is given by the following two-dimensional system

$$\frac{d}{dt}\begin{bmatrix} x \\ y \end{bmatrix} = A(r)\begin{bmatrix} x \\ y \end{bmatrix}, \tag{7}$$

where $r^2 = x^2 + y^2$ and

$$A(r) = \begin{bmatrix} \Lambda(r) & -\Omega(r) \\ \Omega(r) & \Lambda(r) \end{bmatrix}.$$

Such systems are called Omega-Lambda systems (Keener and Sneyd, 2005) and they are special because if we change to polar coordinates, $x = r\cos\theta$, $y = r\sin\theta$, then the ODEs are given by

$$\frac{dr}{dt} = r\Lambda(r) \qquad \text{and} \qquad \frac{d\theta}{dt} = \Omega(r). \tag{8}$$

Assume that $r^* > 0$ is such that $\Lambda(r^*) = 0$. Then this system has a limit cycle which is a perfect circle in $\mathbb{R}^2$ with radius r^* and center at the origin. Let $f'(r)$ denote the derivative of function $f(r)$ with respect to r. If we have

$$\Lambda'(r^*) < 0. \tag{9}$$

then the limit cycle (circle of radius r^*) is stable. Hence this system is an example of a self-sustained stable oscillator whose natural frequency is $\omega_0 = \Omega(r^*)$.

We now introduce noise into the dynamics. We assume that the function $\Omega(r)$ is *noisy*, and we substitute this function in (7) by

$$\Omega(r) + \sigma\xi(t),$$

where σ is the noise-intensity and $\xi(t)$ is the *white-noise* process. Now the dynamics is described by

$$\frac{d}{dt}\begin{bmatrix} x \\ y \end{bmatrix} = A(r)\begin{bmatrix} x \\ y \end{bmatrix} + \sigma N(t)\begin{bmatrix} x \\ y \end{bmatrix}, \tag{10}$$

where $N(t)$ is the 2×2 noise matrix given by

$$N(t) = \begin{bmatrix} 0 & -\xi(t) \\ \xi(t) & 0 \end{bmatrix}.$$

We now discuss the effect of noise on the radius of the limit cycle. We apply Ito's formula (Øksendal, 2003) on

$$r(t) = \sqrt{(x(t))^2 + (y(t))^2}$$

to get

$$\frac{dr}{dt} = r\left(\Lambda(r) + \frac{\sigma^2}{2}\right). \tag{11}$$

Note that even though $x(t)$ and $y(t)$ are noisy signals, $r(t)$ is deterministic. From now on we assume that there exists a r^* such that

$$\Lambda(r^*) = -\frac{\sigma^2}{2} \tag{12}$$

and (9) holds at this r^*. This ensures that the circle with radius r^* centered at the origin is a stable limit cycle for the noisy system (10). Note that Equation (11) shows that we have noise into the dynamics in such a way that it only affects the motion in the direction which is tangential to the limit cycle (θ component) and it does not affect the motion in the direction which is normal to the limit cycle (r component). In general noise may be present in both the components but the noise in the r component may not play a significant role due to the stability of the limit cycle.

Let $(x_0(t), y_0(t))$ be a solution of the system (10). We now examine the dynamics of $(\overline{x}_0(t), \overline{y}_0(t)) = (\mathbb{E}(x_0(t)), \mathbb{E}(y_0(t)))$, where $\mathbb{E}$ denotes the expectation operator. Taking expectation in (10) we get

$$\frac{d}{dt}\begin{bmatrix} \overline{x}_0(t) \\ \overline{y}_0(t) \end{bmatrix} = \frac{d}{dt}\begin{bmatrix} \mathbb{E}(x_0(t)) \\ \mathbb{E}(y_0(t)) \end{bmatrix} = A(r^*)\begin{bmatrix} \overline{x}_0(t) \\ \overline{y}_0(t) \end{bmatrix}, \tag{13}$$

where we have used the fact that $r(t) \approx r^*$ for large values of t. Recall that $\omega_0 = \Omega(r^*)$ is the natural frequency of the oscillator. Note that the 2×2 matrix

$$A(r^*) = \begin{bmatrix} -\frac{\sigma^2}{2} & -\omega_0 \\ \omega_0 & -\frac{\sigma^2}{2} \end{bmatrix}, \tag{14}$$

has eigenvalues

$$-\frac{\sigma^2}{2} \pm i\omega_0$$

where $i = \sqrt{-1}$. Since the real part of both these eigenvalues is negative, the solution of the linear system (13) is such that both $(\overline{x}_0(t)$ and $\overline{y}_0(t))$ undergo damped oscillations (with frequency ω_0) that eventually converge to 0 as $t \to \infty$ (see Figure S4C). In other words we have

$$(\overline{x}_0(t), \overline{y}_0(t)) \to (0, 0) \qquad as \qquad t \to \infty. \tag{15}$$

This behavior is quite unlike the *noise-free* system (7) where the solutions are consistently oscillating with frequency ω_0.
Another way to understand the result (15) is by examining the angular component $\theta(t)$ of the signal $(x_0(t), y_0(t))$. Define

$$\theta(t) = \arctan\left(\frac{y_0(t)}{x_0(t)}\right).$$

Then using Ito's formula we get

$$\frac{d\theta}{dt} = \Omega(r) + \sigma\xi(t). \tag{16}$$

For large values of t, we have $r(t) \approx r^*$ and solving this SDE yields

$$\theta(t) - \omega_0 t = \phi_0(t) = \theta_0 + \sigma B(t), \tag{17}$$

where $\theta_0 = \theta(0)$ is the initial phase and $B(t)$ is the standard Brownian motion (Øksendal, 2003). Note that $\sigma B(t)$ represents the *noise-induced phase-diffusion* term that has been extensively studied in many papers (Pikovsky et al., 2000). Properties of the Brownian motion $B(t)$ imply that $\phi_0(t)$ has the Normal distribution with mean θ_0 and variance $\sigma^2 t$. As t gets large, the variance grows without bounds which implies that the distribution of $\phi_0(t)/2\pi$ ($\phi_0(t)$ modulo 2π) is almost uniform over the interval $[0, 2\pi]$. In Figure S4A we show five trajectories of ϕ_0 and in Figure S4B we illustrate the uniformity of the distribution of $\phi_0(t)/2\pi$ for large values of t.

The above analysis shows that for large t, the single-cell dynamics $(x_0(t), y_0(t))$ is approximately given by

$$\begin{bmatrix} x_0(t) \\ y_0(t) \end{bmatrix} = r^* \begin{bmatrix} \cos(\omega_0 t + \phi_0(t)) \\ \sin(\omega_0 t + \phi_0(t)) \end{bmatrix} = r^* \begin{bmatrix} \cos(\omega_0 t + \theta_0 + \sigma B(t)) \\ \sin(\omega_0 t + \theta_0 + \sigma B(t)) \end{bmatrix}. \tag{18}$$

This representation allows us to easily see that (15) is a direct consequence of the phase-diffusion phenomenon. As explained before, this phenomena causes the distribution of $\phi_0(t)/2\pi$ to be almost uniform over the interval $[0, 2\pi]$, and since *Sine* and *Cosine* are periodic functions with period 2π, we have

$$\bar{x}_0(t) = \mathbb{E}(x_0(t)) \approx \frac{1}{2\pi} \int_0^{2\pi} r^* \cos(\omega_0 t + u) du = 0$$

$$\text{and} \quad \bar{y}_0(t) = \mathbb{E}(y_0(t)) \approx \frac{1}{2\pi} \int_0^{2\pi} r^* \sin(\omega_0 t + u) du = 0 \tag{19}$$

for large values of t, which again proves (15). Such a behavior is consistent with the existing theoretical results on noisy oscillators (Gupta et al., 2014), as well as certain computational and experimental studies on uncoupled circadian clocks with noisy dynamics (Bagheri et al., 2008; To et al., 2007; Ohta et al., 2005; Welsh et al., 1995; Aton et al., 2005).

Self-Sustained Oscillators under Weak Periodic Forcing

We now add weak periodic forcing to the noisy single-cell dynamics (10). This forcing has frequency $\boldsymbol{\omega_f}$ and strength $\boldsymbol{\varepsilon}$, where $\boldsymbol{\varepsilon}$ is a small positive number. The dynamics of the forced system is given by

$$\frac{d}{dt} \begin{bmatrix} x \\ y \end{bmatrix} = A(r) \begin{bmatrix} x \\ y \end{bmatrix} + \sigma N(t) \begin{bmatrix} x \\ y \end{bmatrix} + \varepsilon \begin{bmatrix} \cos(\omega_f t) \\ \sin(\omega_f t) \end{bmatrix}. \tag{20}$$

Let $(x_\varepsilon, y_\varepsilon)$ be a solution of (20). We now use *perturbation theory* to obtain an approximation of $(x_\varepsilon, y_\varepsilon)$ which is accurate up to order ε. In other words, we assume that $(x_\varepsilon, y_\varepsilon)$ has the form

$$\begin{bmatrix} x_\varepsilon \\ y_\varepsilon \end{bmatrix} = \begin{bmatrix} x_0 \\ y_0 \end{bmatrix} + \varepsilon \begin{bmatrix} x_1 \\ y_1 \end{bmatrix} + O(\varepsilon^2). \tag{21}$$

Letting $\varepsilon \to 0$ above we see that (x_0, y_0) must be a solution of (10). Substituting the form (21) in (20) we get

$$\frac{d}{dt} \begin{bmatrix} x_0 \\ y_0 \end{bmatrix} + \varepsilon \frac{d}{dt} \begin{bmatrix} x_1 \\ y_1 \end{bmatrix} = A(r_\varepsilon) \begin{bmatrix} x_0 \\ y_0 \end{bmatrix} + \varepsilon A(r_\varepsilon) \begin{bmatrix} x_1 \\ y_1 \end{bmatrix} + \sigma N(t) \begin{bmatrix} x_0 \\ y_0 \end{bmatrix} + \varepsilon \sigma N(t) \begin{bmatrix} x_1 \\ y_1 \end{bmatrix} + \varepsilon \begin{bmatrix} \cos(\omega_f t) \\ \sin(\omega_f t) \end{bmatrix} + O(\varepsilon^2), \tag{22}$$

where $r_\varepsilon(t) = \sqrt{x_\varepsilon^2(t) + y_\varepsilon^2(t)}$. Since $r_0(t) = \sqrt{x_0^2(t) + y_0^2(t)}$, using (21) we can write

$$r_\varepsilon(t) = r_0(t) + \varepsilon \frac{x_0(t)x_1(t) + y_0(t)y_1(t)}{r_0(t)} + O(\varepsilon^2). \tag{23}$$

Substituting this expression in (22) and using the fact that (x_0, y_0) is the solution to (10), one can see that (x_1, y_1) solves

$$\frac{d}{dt} \begin{bmatrix} x_1 \\ y_1 \end{bmatrix} = A(r_0) \begin{bmatrix} x_1 \\ y_1 \end{bmatrix} + \sigma N(t) \begin{bmatrix} x_1 \\ y_1 \end{bmatrix} + \begin{bmatrix} \cos(\omega_f t) \\ \sin(\omega_f t) \end{bmatrix} + M(x_0, y_0) \begin{bmatrix} x_1 \\ y_1 \end{bmatrix},$$

where $M(x_0, y_0)$ is the 2×2 matrix given by

$$M(x_0, y_0) = \frac{1}{r_0} \begin{bmatrix} \Lambda'(r_0)x_0^2 - \Omega'(r_0)x_0y_0 & \Lambda'(r_0)x_0y_0 - \Omega'(r_0)y_0^2 \\ \Lambda'(r_0)x_0y_0 + \Omega'(r_0)x_0^2 & \Omega'(r_0)x_0y_0 + \Lambda'(r_0)y_0^2 \end{bmatrix}.$$

Note that for large values of t, we have $r_0(t) \approx r^*$, $\omega_0 = \Omega(r^*)$ and $\Lambda(r^*) = -\sigma^2/2$. For simplicity, we assume $\Omega'(r^*) = 0$ from now on. Hence the long-term dynamics of (x_1, y_1) simplifies to:

$$\frac{d}{dt}\begin{bmatrix} x_1 \\ y_1 \end{bmatrix} = \begin{bmatrix} -\frac{\sigma^2}{2} & -\omega_0 \\ \omega_0 & -\frac{\sigma^2}{2} \end{bmatrix}\begin{bmatrix} x_1 \\ y_1 \end{bmatrix} + \sigma N(t)\begin{bmatrix} x_1 \\ y_1 \end{bmatrix} + \begin{bmatrix} \cos(\omega_f t) \\ \sin(\omega_f t) \end{bmatrix} + \frac{\Lambda'(r^*)}{r^*}\begin{bmatrix} x_0^2 & x_0 y_0 \\ x_0 y_0 & y_0^2 \end{bmatrix}\begin{bmatrix} x_1 \\ y_1 \end{bmatrix}. \tag{24}$$

For any (x_0, y_0) of the form (18), let $P_{(x_0,y_0)} : \mathbb{R}^2 \to \mathbb{R}^2$ be the projection map given by

$$P_{(x_0,y_0)}(x,y) = \left(\frac{x x_0 + y y_0}{x_0^2 + y_0^2}\right)(x_0, y_0) = \frac{\langle (x,y), (x_0,y_0)\rangle}{\langle (x_0,y_0), (x_0,y_0)\rangle}(x_0, y_0) = \frac{\langle (x,y), (x_0,y_0)\rangle}{(r^*)^2}(x_0, y_0),$$

where $\langle \cdot, \cdot \rangle$ denotes the standard inner product on $\mathbb{R}^2$. Note that $P_{(x_0,y_0)}(x,y)$ gives the component of the vector (x,y) in the direction (x_0, y_0). One can view the linear transformation $P_{(x_0,y_0)}$ as the 2×2 matrix

$$\overline{P}_{(x_0,y_0)} = \frac{1}{(r^*)^2}\begin{bmatrix} x_0^2 & x_0 y_0 \\ x_0 y_0 & y_0^2 \end{bmatrix},$$

in the sense that for any $(x,y) \in \mathbb{R}^2$ we have that

$$P_{(x_0,y_0)}(x,y) = \overline{P}_{(x_0,y_0)}\begin{bmatrix} x \\ y \end{bmatrix}.$$

Hence Equation (24) simplifies to

$$\frac{d}{dt}\begin{bmatrix} x_1 \\ y_1 \end{bmatrix} = \begin{bmatrix} -\frac{\sigma^2}{2} & -\omega_0 \\ \omega_0 & -\frac{\sigma^2}{2} \end{bmatrix}\begin{bmatrix} x_1 \\ y_1 \end{bmatrix} + \sigma N(t)\begin{bmatrix} x_1 \\ y_1 \end{bmatrix} + \begin{bmatrix} \cos(\omega_f t) \\ \sin(\omega_f t) \end{bmatrix} + \Lambda'(r^*) r^* \overline{P}_{(x_0,y_0)}\begin{bmatrix} x_1 \\ y_1 \end{bmatrix}. \tag{25}$$

Let

$$\alpha(t) = \frac{x_0(t)x_1(t) + y_0(t)y_1(t)}{(r^*)^2} = \frac{\langle (x_1(t), y_1(t)), (x_0(t), y_0(t))\rangle}{(r^*)^2}, \tag{26}$$

and note that

$$\overline{P}_{(x_0(t),y_0(t))}\begin{bmatrix} x_1(t) \\ y_1(t) \end{bmatrix} = \alpha(t)\begin{bmatrix} x_0(t) \\ y_0(t) \end{bmatrix}. \tag{27}$$

Using Ito's formula we obtain the equation for $\alpha(t)$ as

$$\frac{d\alpha}{dt} = \frac{x_0(t)\cos(\omega_f t) + y_0(t)\sin(\omega_f t)}{(r^*)^2} + \Lambda'(r^*) r^* \alpha(t). \tag{28}$$

Note that $\Lambda'(r^*) < 0$ (9) and its absolute value $|\Lambda'(r^*)|$ can be seen as the *stability strength* of the oscillator. Using (18) and solving the equation for $\alpha(t)$ yields

$$\alpha(t) = \alpha(0) e^{-|\Lambda'(r^*)| r^* t} + \frac{1}{r^*}\int_0^t e^{-(|\Lambda'(r^*)| r^*)(t-s)} \cos((\omega_0 - \omega_f)s + \theta_0 + \sigma B(s))ds.$$

Note that $\alpha(t)$ is a finite *total variation* process (Øksendal, 2003), and since the Cosine function is bounded between -1 and 1, the absolute value of $\alpha(t)$ can be bounded above by

$$|\alpha(t)| \leq \frac{1}{|\Lambda'(r^*)|\,(r^*)^2}. \tag{29}$$

Define $(x_f(t), y_f(t))$ as

$$\begin{bmatrix} x_f(t) \\ y_f(t) \end{bmatrix} = \begin{bmatrix} x_1(t) \\ y_1(t) \end{bmatrix} - \alpha(t)\begin{bmatrix} x_0(t) \\ y_0(t) \end{bmatrix} = \left(I - \overline{P}_{(x_0(t),y_0(t))}\right)\begin{bmatrix} x_1(t) \\ y_1(t) \end{bmatrix}, \tag{30}$$

where I is the 2×2 identity matrix. Observe that $(x_f(t), y_f(t))$ gives the component of $(x_1(t), y_1(t))$ that is *tangential* to the limit cycle at $(x_0(t), y_0(t))$. Using (10) and (25), we can derive the equation for $(x_f(t), y_f(t))$ as below:

$$\frac{d}{dt}\begin{bmatrix} x_f \\ y_f \end{bmatrix} = \frac{d}{dt}\begin{bmatrix} x_1 \\ y_1 \end{bmatrix} - \alpha(t)\frac{d}{dt}\begin{bmatrix} x_0 \\ y_0 \end{bmatrix} - \begin{bmatrix} x_0 \\ y_0 \end{bmatrix}\frac{d\alpha}{dt} = \begin{bmatrix} -\frac{\sigma^2}{2} & -\omega_0 \\ \omega_0 & -\frac{\sigma^2}{2} \end{bmatrix}\begin{bmatrix} x_f \\ y_f \end{bmatrix} + \sigma N(t)\begin{bmatrix} x_f \\ y_f \end{bmatrix} + \begin{bmatrix} \cos(\omega_f t) \\ \sin(\omega_f t) \end{bmatrix} + \Lambda'(r^*) r^* \overline{P}_{(x_0,y_0)}\begin{bmatrix} x_1 \\ y_1 \end{bmatrix} - \begin{bmatrix} x_0 \\ y_0 \end{bmatrix}\frac{d\alpha}{dt}.$$

However (27) and (28) imply that

$$\Lambda'(r^*) r^* \overline{P}_{(x_0,y_0)}\begin{bmatrix} x_1 \\ y_1 \end{bmatrix} - \begin{bmatrix} x_0 \\ y_0 \end{bmatrix}\frac{d\alpha}{dt} = \Lambda'(r^*) r^* \alpha(t)\begin{bmatrix} x_0 \\ y_0 \end{bmatrix} - \Lambda'(r^*) r^* \alpha(t)\begin{bmatrix} x_0 \\ y_0 \end{bmatrix} - \overline{P}_{(x_0,y_0)}\begin{bmatrix} \cos(\omega_f t) \\ \sin(\omega_f t) \end{bmatrix} = -\overline{P}_{(x_0,y_0)}\begin{bmatrix} \cos(\omega_f t) \\ \sin(\omega_f t) \end{bmatrix}.$$

Hence the equation for $(x_f(t), y_f(t))$ simplifies to

$$\frac{d}{dt}\begin{bmatrix} x_f \\ y_f \end{bmatrix} = \begin{bmatrix} -\frac{\sigma^2}{2} & -\omega_0 \\ \omega_0 & -\frac{\sigma^2}{2} \end{bmatrix}\begin{bmatrix} x_f \\ y_f \end{bmatrix} + \sigma N(t)\begin{bmatrix} x_f \\ y_f \end{bmatrix} + \left(I - \overline{P}_{(x_0,y_0)}\right)\begin{bmatrix} \cos(\omega_f t) \\ \sin(\omega_f t) \end{bmatrix}. \tag{31}$$

The drift and diffusion components of this SDE are growing at most linearly in (x_f, y_f), and the forcing term is bounded. Therefore using the classical existence and uniqueness result for SDEs (see for e.g., Theorem 5.2.1 in (Øksendal, 2003)) we can see that its solution is well-defined in any finite time interval $[0, T]$. Moreover on such a time interval we have

$$\mathbb{E}\left[\int_0^T \left(x_f^2(t) + y_f^2(t)\right) dt\right] < \infty \tag{32}$$

which shows that this solution is well-behaved and does not grow unboundedly.

Since $(x_0(t), y_0(t))$ is given by (18), we can write the matrix $\overline{P}_{(x_0,y_0)}$ as

$$\overline{P}_{(x_0,y_0)} = \frac{1}{(r^*)^2}\begin{bmatrix} x_0^2 & x_0 y_0 \\ x_0 y_0 & y_0^2 \end{bmatrix} = \begin{bmatrix} \cos^2(\omega_0 t + \phi_0(t)) & \sin(\omega_0 t + \phi_0(t))\cos(\omega_0 t + \phi_0(t)) \\ \sin(\omega_0 t + \phi_0(t))\cos(\omega_0 t + \phi_0(t)) & \sin^2(\omega_0 t + \phi_0(t)) \end{bmatrix}.$$

We now examine the dynamics of $(\overline{x}_f(t), \overline{y}_f(t)) = (\mathbb{E}(x_f(t)), \mathbb{E}(y_f(t)))$, where $\mathbb{E}$ denotes the expectation operator. Taking expectation in (31) we get

$$\frac{d}{dt}\begin{bmatrix} \overline{x}_f(t) \\ \overline{y}_f(t) \end{bmatrix} = \frac{d}{dt}\begin{bmatrix} \mathbb{E}(x_f(t)) \\ \mathbb{E}(y_f(t)) \end{bmatrix} = \begin{bmatrix} -\frac{\sigma^2}{2} & -\omega_0 \\ \omega_0 & -\frac{\sigma^2}{2} \end{bmatrix}\begin{bmatrix} \overline{x}_f(t) \\ \overline{y}_f(t) \end{bmatrix} + \left(I - \mathbb{E}\left(\overline{P}_{(x_0(t),y_0(t))}\right)\right)\begin{bmatrix} \cos(\omega_f t) \\ \sin(\omega_f t) \end{bmatrix}. \tag{33}$$

Recall that for large t, the distribution of $\phi_0(t)/2\pi$ is almost uniform over the interval $[0, 2\pi]$. Therefore the expectation of this matrix can be computed as

$$\mathbb{E}\left(\overline{P}_{(x_0,y_0)}\right) = \frac{1}{2\pi}\begin{bmatrix} \int_0^{2\pi} \cos^2(\omega_0 t + u)du & \int_0^{2\pi} \sin(\omega_0 t + u)\cos(\omega_0 t + u)du \\ \int_0^{2\pi} \sin(\omega_0 t + u)\cos(\omega_0 t + u)du & \int_0^{2\pi} \sin^2(\omega_0 t + u)du \end{bmatrix} = \begin{bmatrix} \frac{1}{2} & 0 \\ 0 & \frac{1}{2} \end{bmatrix}.$$

Substituting this expectation and solving the linear system (33) we get

$$\begin{aligned} \begin{bmatrix} \overline{x}_f(t) \\ \overline{y}_f(t) \end{bmatrix} &= e^{-\frac{\sigma^2}{2}t}\begin{bmatrix} \cos(\omega_0 t) & -\sin(\omega_0 t) \\ \sin(\omega_0 t) & \cos(\omega_0 t) \end{bmatrix}\begin{bmatrix} \overline{x}_f(0) \\ \overline{y}_f(0) \end{bmatrix} + \frac{1}{2}\int_0^t e^{-\frac{\sigma^2}{2}(t-s)}\begin{bmatrix} \cos(\omega_0(t-s)) & -\sin(\omega_0(t-s)) \\ \sin(\omega_0(t-s)) & \cos(\omega_0(t-s)) \end{bmatrix}\begin{bmatrix} \cos(\omega_f s) \\ \sin(\omega_f s) \end{bmatrix} ds \\ &= e^{-\frac{\sigma^2}{2}t}\begin{bmatrix} \cos(\omega_0 t) & -\sin(\omega_0 t) \\ \sin(\omega_0 t) & \cos(\omega_0 t) \end{bmatrix}\begin{bmatrix} \overline{x}_f(0) \\ \overline{y}_f(0) \end{bmatrix} + \frac{1}{2}\int_0^t e^{-\frac{\sigma^2}{2}(t-s)}\begin{bmatrix} \cos(\omega_0(t-s) + \omega_f s) \\ \sin(\omega_0(t-s) + \omega_f s) \end{bmatrix} ds. \end{aligned} \tag{34}$$

Let A_0 and A_f be constants given by

$$A_0 = \sqrt{(\overline{x}_f(0))^2 + (\overline{y}_f(0))^2} \quad \text{and} \quad A_f = \frac{1}{\sqrt{(\omega_0 - \omega_f)^2 + \left(\frac{\sigma^2}{2}\right)^2}}.$$

Also define to be ϕ_0 and ϕ_f^* be angles whose *Sine* and *Cosine* values are as follows

$$\cos(\phi_0)=\frac{\overline{x}_f(0)}{A_0},\quad \sin(\phi_0)=\frac{\overline{y}_f(0)}{A_0},\quad \cos(\phi_f^*)=\frac{\frac{\sigma^2}{2}}{A_f},\quad \textit{and}\quad \sin(\phi_f^*)=\frac{\omega_0-\omega_f}{A_f}.$$

Upon evaluating the integral in (34), the formula for $(\overline{x}_f(t),\overline{y}_f(t))$ simplifies to

$$\begin{bmatrix}\overline{x}_f(t)\\ \overline{y}_f(t)\end{bmatrix}=A_0e^{-\frac{\sigma^2}{2}t}\begin{bmatrix}\cos(\omega_0t+\phi_0)\\ \sin(\omega_0t+\phi_0)\end{bmatrix}+\frac{A_f}{2}\begin{bmatrix}\cos(\omega_ft+\phi_f^*)\\ \sin(\omega_ft+\phi_f^*)\end{bmatrix}-\frac{A_f}{2}e^{-\frac{\sigma^2}{2}t}\begin{bmatrix}\cos(\omega_0t+\phi_f^*)\\ \sin(\omega_0t+\phi_f^*)\end{bmatrix}. \tag{35}$$

In the presence of dynamical noise $(\sigma>0)$ the long-term dynamics of $(\overline{x}_f(t),\overline{y}_f(t))$ can be approximated by

$$\begin{bmatrix}\overline{x}_f(t)\\ \overline{y}_f(t)\end{bmatrix}=\frac{A_f}{2}\begin{bmatrix}\cos(\omega_ft+\phi_f^*)\\ \sin(\omega_ft+\phi_f^*)\end{bmatrix}, \tag{36}$$

which shows that $(\overline{x}_f(t),\overline{y}_f(t))$ oscillates with the forcing frequency ω_f and has no component that oscillates with the natural frequency ω_0. This agrees with the main finding of our paper which claims that noise in the dynamics facilitates entrainment of the population-averaged signal. We now consider the case when there is no noise in the dynamics of individual cells $(\sigma=0)$. In such a scenario $(x_f(t),y_f(t))$ and $(\overline{x}_f(t),\overline{y}_f(t))$ coincide and they can be expressed as

$$\begin{bmatrix}x_f(t)\\ y_f(t)\end{bmatrix}=A_0\begin{bmatrix}\cos(\omega_0t+\phi_0)\\ \sin(\omega_0t+\phi_0)\end{bmatrix}+\frac{A_f}{2}\begin{bmatrix}\cos(\omega_ft+\phi_f^*)\\ \sin(\omega_ft+\phi_f^*)\end{bmatrix}-\frac{A_f}{2}\begin{bmatrix}\cos(\omega_0t+\phi_f^*)\\ \sin(\omega_0t+\phi_f^*)\end{bmatrix}. \tag{37}$$

This deterministic signal is clearly not entrained because it has a non-trivial component which oscillates with frequency ω_0. One may wonder if we can recover entrainment at the population-level just by randomizing the initial phase ϕ_0 rather than introducing dynamical noise. To investigate this issue we keep $\sigma=0$, but let ϕ_0 be a $[0,2\pi]$-valued random variable with probability distribution Φ_0. This random variable ϕ_0 assumes different values for different cells, allowing the population-level behavior to be different from the behavior of a single-cell, even though the dynamics is deterministic. The population-level signal is now given by $(\overline{x}_f(t),\overline{y}_f(t))=(\mathbb{E}_{\Phi_0}(x_f(t)),\mathbb{E}_{\Phi_0}(y_f(t)))$, where $\mathbb{E}_{\Phi_0}$ denotes the expectation w.r.t. probability distribution Φ_0. From (37) it is immediate that

$$\begin{bmatrix}\overline{x}_f(t)\\ \overline{y}_f(t)\end{bmatrix}=\begin{bmatrix}\mathbb{E}_{\Phi_0}(x_f(t))\\ \mathbb{E}_{\Phi_0}(y_f(t))\end{bmatrix}=A_0\begin{bmatrix}\mathbb{E}_{\Phi_0}(\cos(\omega_0t+\phi_0))\\ \mathbb{E}_{\Phi_0}(\sin(\omega_0t+\phi_0))\end{bmatrix}+\frac{A_f}{2}\begin{bmatrix}\cos(\omega_ft+\phi_f^*)\\ \sin(\omega_ft+\phi_f^*)\end{bmatrix}-\frac{A_f}{2}\begin{bmatrix}\cos(\omega_0t+\phi_f^*)\\ \sin(\omega_0t+\phi_f^*)\end{bmatrix}.$$

The last term in this equation is non-trivial and it oscillates with frequency ω_0 indicating that this population-level signal $(\overline{x}_f(t),\overline{y}_f(t))$ will not be entrained *for any choice* of initial phase distribution Φ_0. In particular, even when Φ_0 has uniform distribution over $[0,2\pi]$, the first term in this equation will disappear (recall (19)) but the last term still remains ensuring that $(\overline{x}_f(t),\overline{y}_f(t))$ is not entrained. The same issue does not arise in the stochastic case $(\sigma>0)$ because the long-term dynamics (36) is unaffected by the initial phase distribution. This agrees with the observation we made earlier that in the stochastic case, randomizing the initial phases of cells does not significantly affect the population-level Arnol'd Tongue.

Another way to understand the above result is by studying the dynamics of the angular-variable $\theta_f(t)$ corresponding to the system (31). Define

$$\theta_f(t)=\arctan\left(\frac{y_f(t)}{x_f(t)}\right).$$

Then using Ito's formula we get

$$\frac{d\theta_f}{dt}=\omega_0+\sigma\xi(t)-\frac{1}{2r_f(t)}\sin(\theta_f(t)-\omega_ft)+\frac{1}{2r_f(t)}\sin(\theta_f(t)+\omega_ft-2\omega_0t-2\phi_0(t)),$$

where

$$r_f(t)=\sqrt{x_f^2(t)+y_f^2(t)}.$$

Letting

$$\phi_f(t)=\theta_f(t)-\omega_ft, \tag{38}$$

to be the phase variable we obtain

$$\frac{d\phi_f}{dt}=\omega_0-\omega_f+\sigma\xi(t)-\frac{1}{2r_f(t)}\sin(\phi_f(t))+\frac{1}{2r_f(t)}\sin(\phi_f(t)-2(\omega_0-\omega_f)t-2\phi_0(t)). \tag{39}$$

Note that $\phi_f(t)$ measures the difference between the angle $\theta_f(t)$ of the system (31) and the angle of the forcing input $\omega_f t$. Equations similar to (39) are known to describe the dynamics of this phase for more general examples (Pikovsky et al., 2000, 2001). Assuming that the frequency mismatch or *detuning* factor $|\omega_0 - \omega_f|$ is small, the process ϕ_f behaves like a mean-reverting Ornstein-Uhlenbeck process (Øksendal, 2003) given by

$$\frac{d\phi}{dt} = -(\phi - \phi^*) + \sigma\xi(t), \tag{40}$$

where ϕ^* is some constant. Properties of such a process imply as t tends to infinity, the random variable $\phi(t)$ converges in distribution to a Normal random variable with mean ϕ^* and a bounded variance. This suggests that for large values of t, the distribution of $\phi_f(t)/2\pi$ is *concentrated* over a small region in the interval $[0, 2\pi]$, which is very different from the constant-environment situation where the distribution was uniform. Note that $(x_f(t), y_f(t))$ can be expressed as

$$\begin{bmatrix} x_f(t) \\ y_f(t) \end{bmatrix} = r_f(t) \begin{bmatrix} \cos(\omega_f t + \phi_f(t)) \\ \sin(\omega_f t + \phi_f(t)) \end{bmatrix}. \tag{41}$$

From the concentrated nature of the distribution of $\phi_f(t)/2\pi$, one can verify that the expected signal $(\overline{x}_f(t)), (\overline{y}_f(t)) = (\mathbb{E}(x_f(t)), \mathbb{E}(y_f(t)))$ is oscillatory with frequency ω_f, as proved by (36). Observe that the expected signal does not vanish as $t \to \infty$, as in the constant-environment situation (19).

Combining (18), (21), (30) and (41) we see that for large t, the solution of the weakly forced noisy self-sustained oscillator (20) is of the form:

$$\begin{aligned} \begin{bmatrix} x_\varepsilon(t) \\ y_\varepsilon(t) \end{bmatrix} &= \begin{bmatrix} x_0(t) \\ y_0(t) \end{bmatrix} + \varepsilon \begin{bmatrix} x_1(t) \\ y_1(t) \end{bmatrix} + O(\varepsilon^2) \\ = r^*(1 + \varepsilon\alpha(t)) &\begin{bmatrix} \cos(\omega_0 t + \phi_0(t)) \\ \sin(\omega_0 t + \phi_0(t)) \end{bmatrix} + \varepsilon r_f(t) \begin{bmatrix} \cos(\omega_f t + \phi_f(t)) \\ \sin(\omega_f t + \phi_f(t)) \end{bmatrix} + O(\varepsilon^2), \end{aligned} \tag{42}$$

where $\alpha(t)$ is given by (26). Moreover the distribution of $\phi_0(t)/2\pi$ ($\phi_0(t)$ modulo 2π) is almost uniform over the interval $[0, 2\pi]$ while the distribution of $\phi_f(t)/2\pi$ is concentrated over a small region in the interval $[0, 2\pi]$. Representation (42) describes the single-cell dynamics in this *weak* periodic input case, as a superposition of two signals: a *strong* signal (18) with frequency ω_0 (natural frequency) and a *weak* signal (41) with frequency ω_f (forcing frequency).

As mentioned in the main paper, using (42) we can easily explain our main findings. If we *turn-off* the noise, then $\phi_0(t)$ and $\phi_f(t)$ become deterministic constants, and the resulting deterministic signal is oscillatory with a frequency which is very different from the forcing frequency ω_f. In fact the majority of the signal power lies at the natural frequency ω_0, indicating that the dynamics is *not entrained* by the weak periodic input. When noise enters the dynamics, $\phi_0(t)$ and $\phi_f(t)$ become random variables, causing cell to cell heterogeneity. The single-cell trajectories exhibit oscillations, but they lack coherence due to noise. As in the deterministic case, a single-cell signal also attributes most of its power at the natural frequency ω_0, thereby showing that the signal is again *not entrained* by the weak periodic input. However the entrainment property emerges at the population-level when we consider the signal $(\overline{x}_\varepsilon(t), \overline{y}_\varepsilon(t)) = (\mathbb{E}(x_\varepsilon(t)), \mathbb{E}(y_\varepsilon(t)))$ formed by taking the average of several single-cell signals. To see this effect observe that (15) and (36) imply that for large values of t

$$\overline{x}_\varepsilon(t) := \mathbb{E}(x_\varepsilon(t)) \approx \varepsilon\left(\frac{A_f}{2}\right)\cos\left(\omega_f t + \phi_f^*\right) + \varepsilon \int_{-\overline{\alpha}}^{\overline{\alpha}} \int_0^{2\pi} a\cos(\omega_0 t + z) G(a,z) dz da + O\left(\varepsilon^2\right),$$

and

$$\overline{y}_\varepsilon(t) := \mathbb{E}(y_\varepsilon(t)) \approx \varepsilon\left(\frac{A_f}{2}\right)\sin\left(\omega_f t + \phi_f^*\right) + \varepsilon \int_{-\overline{\alpha}}^{\overline{\alpha}} \int_0^{2\pi} a\sin(\omega_0 t + z) G(a,z) dz da + O\left(\varepsilon^2\right),$$

where $G(a,z)$ is the joint distribution function of $(r^*\alpha(t))$ and $\varphi_0(t)/2\pi$. Note that $r^*\alpha(t)$ is bounded above by

$$\overline{\alpha} = \frac{1}{|\Lambda'(r^*)|r^*}$$

due to (29). In average or expectation, the dominant term in (42) corresponding to the natural frequency ω_0 drops out because of the uniformity of the distribution of $\phi_0(t)/2\pi$ as before in (19). Hence only the terms of order ε remain in $(\overline{x}_\varepsilon(t), \overline{y}_\varepsilon(t))$, making it possible for the majority of this signal's power to lie at the forcing frequency ω_f. This is because this signal includes the signal $(\overline{x}_f(t), \overline{y}_f(t)) = (\mathbb{E}(x_f(t)), \mathbb{E}(y_f(t)))$ (see (36)) which oscillates with frequency ω_f. Therefore the population-level signal $(\overline{x}_\varepsilon(t), \overline{y}_\varepsilon(t))$ can become *well-entrained* to the weak periodic input even though the single-cell signals are not. Furthermore, we can also conclude that this population-level entrainment is *facilitated* by the noise because if we remove the noise, then the resulting deterministic system is *not entrained* by the weak periodic input, as explained above. We end this section by noting that when the *stability strength* $|\Lambda'(r^*)|$ of the oscillator is high, then $\overline{\alpha} \approx 0$ and $(\overline{x}_\varepsilon(t), \overline{y}_\varepsilon(t))$ is almost perfectly entrained to the periodic input.

QUANTIFICATION AND STATISTICAL ANALYSIS

In the stochastic setting, we pool together several single-cell trajectories and take their average (at each time-point) we obtain a trajectory that corresponds to the population-level dynamics. All trajectories are analyzed after removing an initial time-period to ensure that the transience has been eliminated. Using the Discrete Fourier Transform (DFT) we compute the Power Spectral Density (PSD) of any trajectory to decide if the dynamics is entrained or not: to be entrained, the power corresponding to the frequency-mode ω_f (and its harmonics) should be a significant percentage of the total signal power. Thereafter by scanning the frequency-amplitude space, the Arnol'd Tongues can be plotted. Note that the DFT of a signal also allows us to evaluate the phase variables ϕ_0 and ϕ_f corresponding to the natural component (frequency ω_0) and the forcing component (frequency ω_f) of the signal. Using these phase realizations from several single-cell trajectories we can plot the histograms for the distributions of ϕ_0 and ϕ_f modulo 2π (see Figure 6). More information on the determination of entrainment and the computation of Arnol'd Tongues is provided below.

Determination of Entrainment

Consider a system that is driven by a periodic forcing signal with frequency ω_f. The output of the system is said to be entrained (Pikovsky et al., 2001) to the forcing signal with a $m:n$ ratio if the output is periodic with a frequency ω_{out} and $\omega_{\text{out}}/\omega_f = m/n$. For the Van der Pol oscillator we only consider $1:1$ entrainment and for the Spiky NF-κ B model and the Circadian Clock we only consider $1:1$ and $1:2$ entrainment.

Spectral Power and Phase

For a specific forcing amplitude $\boldsymbol{u_A}$ and forcing frequency $\boldsymbol{\omega_f}$ let $\boldsymbol{f_j}$ be the samples of the output of the system at time $\boldsymbol{t_j = j \times dt}$ for $\boldsymbol{j \in \{0 \ldots N-1\}}$. We substract the time-average of the signal to get:

$$\tilde{f}_j = f_j - \frac{1}{N}\sum_{m=0}^{N-1} f_m.$$

We compute the discrete fourier transformation (DFT) $\tilde{F}$ of the sequence of samples $\tilde{f}_i$ as:

$$\tilde{F}_k = \sum_{j=0}^{N-1} \tilde{f}_j \nu_{kj},$$

where $\nu_{kj} = \exp(-i\ 2\pi k\ j/N)$ and $k = 0, 1, \ldots, (N-1)$. The spectral power P_k of the output signal at frequency $k/(N \times dt)$ and the corresponding phase ϕ_k are given by

$$P_k = \frac{dt}{N}|\tilde{F}_k|^2 \qquad \textit{and} \qquad \phi_k = \arg\left(\tilde{F}_k\right),$$

where $|z|$ and $\arg(z)$ denote the absolute value and argument of a complex number z.

Note that these P_k-s give us the *Power Spectral Density* (PSD) of the output signal. As we only use ratios of P_k-s later on, the normalization of P_k-s is not important. We use the MATLAB function *fft*. This function applies the Cooley-Tukey algorithm (Cooley and Tukey, 1965) which expects the number of samples N to be a power of 2 and thus we truncate the samples of the output accordingly. As the output is real-valued it follows that $\tilde{F}_{N-k} = \tilde{F}_k^*$ for $k = 0, 1, \ldots, (N/2)$, and thus we only need to evaluate the $\tilde{F}_k$-s for $k = 0, 1, \ldots, (N/2)$.

Entrainment Score

The Fourier transformation of a periodic signal with a period $\boldsymbol{T}$ will be a sum of Dirac-delta distributions located at frequencies $\boldsymbol{\omega = j \times (2\pi/T)}$ **for** $\boldsymbol{j \in \mathbb{N}_0}$, i.e., the power at the fundamental frequency $\boldsymbol{1/T}$ and all the higher harmonics (the component at frequency $\boldsymbol{\omega = 0}$ corresponds to the mean of the signal). We can use this fact to test the entrainment of a system, however, due to the finite observation time and transient-effects in the system dynamics, the spectral power of an entrained system will be spread around the corresponding components of the DFT. To accommodate for this numerical issue, we define a narrow frequency window of width $\boldsymbol{\Delta\nu = 0.01 \times \omega_0}$ and put this window around the fundamental and higher harmonics of the forcing frequency. We can then approximate the spectral power corresponding to the forcing frequency by summing up the spectral power within these windows:

$$P^{\text{in}} = \sum\nolimits_{j=1}^{\infty} \sum_{k \in \mathcal{A}_j} |\tilde{F}_k|^2$$

$$\mathcal{A}_j = \{k : j \cdot \omega_f - \Delta\nu \leq j \cdot \nu_k \leq j \cdot \omega_f + \Delta\nu\},$$

i.e $\mathcal{A}_j$ represents the DFT components within the frequency window around the j^{th} harmonic and P^{in} is the approximate spectral power corresponding to the forcing frequency ω_f. We define the entrainment score as the ratio of the spectral power corresponding to the forcing frequency and the total spectral power as

$$S = \frac{P^{\text{in}}}{P^{\text{total}}} \quad \text{and} \quad P^{\text{total}} = \sum_{k=0}^{N-1} \left| \tilde{F}_k \right|^2.$$

In the case of a deterministic system that is entrained to a periodic forcing signal, the entrainment score S will approach 1 as the observation time $N \times dt$ approaches infinity. Because of this we choose an entrainment threshold S_{ent} that is close to one and call a system entrained if $S \geq S_{\text{ent}}$.

Entrainment for Stochastic Systems

We now discuss how the decision of whether the output of a stochastic system is entrained or not is made. For such systems the notion of entrainment should be based on an ensemble of individual oscillators, i.e., a population of oscillators with identical dynamics but with different realizations of the noise.

To decide the entrainment of a population-level signal we compute the entrainment score based on the average DFT of several single-cell realizations. Due to the linearity of the Fourier transformation this is equivalent to computing the DFT of the average of single-cell signals. To decide entrainment at the single-cell level we compute the entrainment score for each realization of the system. We then define the single-cell level entrainment score to be the average entrainment score of the 50% highest entrainment scores of the individual realizations.

As in the deterministic case, we call the system entrained at the population-level or the single-cell level, if the corresponding entrainment score is higher than the entrainment threshold S_{ent}. Since the entrainment will never be perfect due to the stochasticity in the system as well as numerical errors, we use an entrainment threshold of $S_{\text{ent}} = 0.75$ in all our examples.

Computation of the Arnol'd Tongues

The computation of the Arnol'd Tongues involves a scan over two parameters, the forcing frequency and the forcing amplitude. For each pair of these parameter values many realizations have to be computed for a sufficiently large observation time. This is a very time consuming procedure and to make this computation tractable we make the following assumption: given that u_A^0 is the minimum amplitude for which a system is entrained, i.e., the border of the Arnol'd Tongue, we assume that the system is also entrained for all forcing amplitudes $u_A > u_A^0$, i.e., there are no holes in the Arnol'd Tongues. Note that this assumption is not true in general, and for the systems we consider, the entrainment ratio can change with increasing forcing amplitude. However, we carefully checked that this assumption holds by explicitly testing a few forcing frequencies in each example.

To approximate the Arnol'd Tongue numerically, we choose a finite range of forcing frequencies $\{\omega_f^0, \ldots, \omega_f^M\}$, a maximum forcing amplitude $u_A^{\max}$, and a desired accuracy level for the Arnol'd Tongue border ε^A. With the assumption mentioned above, we can resort to a binary search on the forcing amplitude range $[0, u_A^{\max}]$ to find the minimum forcing amplitude u_A^0 for which the system is entrained for a specific forcing frequency and entrainment ratio. The binary search is performed until u_A^0 is approximated within the desired accuracy of ε^A.

The required SDEs were numerically solved using a custom, parallel implementation of the Euler-Maruyama method in Java (Kloeden and Platen, 1992). This solver is interfaced with MATLAB where we performed all the numerical analysis. Because of the stochastic nature of the dynamics, many trajectories have to be simulated to obtain representative results for the system. On top of this, the system has to be simulated for a considerable amount of time for it to reach stationarity. These issues make the computation of *Arnol'd Tongues* very demanding, even with the simplifying assumption made above. Therefore we performed all computations *in parallel* on the ETH Zurich High Performance Cluster Brutus. To illustrate the computational costs, the computation of the *Arnol'd Tongues* for the Circadian Clock model took a total CPU time of about 700 days.

DATA AND SOFTWARE AVAILABILITY

The data used for generating Figure 1 was provided by Savas Tay (Institute of Molecular Engineering, University of Chicago) and it also appears in (Kellogg and Tay, 2015). All the other data were computationally generated following the procedures mentioned above. The computer code used for generating and analyzing the data may be requested from the authors.